Flow analysis of a heat pump tumble dryer using a general theoretical model

Christofer Svensson

Thesis for the degree of Master of Science in Engineering
Division of Fluid Mechanics
Department of Energy Sciences
Faculty of Engineering | Lund University

Flow analysis of a heat pump tumble dryer using a general theoretical model and CFD simulations

Christofer Svensson

Mars 2018, Lund

This degree project for the degree of Master of Science in Engineering has been conducted at the Division of Fluid Mechanics , Department of Energy Sciences, Faculty of Engineering, Lund University, and at Electrolux Professional AB

Supervisor at the Division of Fluid Mechanics. was Dr Robert Szasz
Supervisor at Electrolux Professional AB was Mikael Blomqvist
Examiner at Lund University was Professor Johan Revstedt

The project was carried out in cooperation with Electrolux Professional AB

Thesis for the Degree of Master of Science in Engineering

ISRN LUTMDN/TMHP-17/5402-SE

ISSN 0282-1990

Fluid Mechanics
Department of Energy Sciences
Faculty of Engineering, Lund University
Box 118, 221 00 Lund
Sweden

www.energy.lth.se

Flow analysis of a heat pump tumble dryer using a general theoretical model and CFD simulations.

Christofer Svensson

Lund University, Faculty of Engineering, Department of Energy Sciences

2017

Abstract (English)

Drying clothes is an essential but energy demanding process in modern society. A common way to dry clothes is tumble drying. Electrolux is one of the world leading manufacturers of household appliances and currently is working on a heat pump tumble dryer product. This master thesis is a study of the aerodynamic properties for the internal air flow for the mentioned heat pump tumble dryer. If pressure losses can be reduced then the energy required for the fan can be lowered. The goal is to identify pressure distribution and potential geometry improvements across the system. The work consisted in building a prototype of a theoretical pressure distribution model, doing CFD simulations inside the heat pump side of the geometry, and one geometry change was tested in CFD and at the lab in Ljungby.

The theoretical model was constructed with laundry load and filter clogging as inputs and pressure distribution as outputs. The model was useful in identifying critical values for load and filter in creating suction in the drum, to help keep the hatch from leaking through its rubber seals.

The CFD was performed at the heat pump side of the system. Results from this was useful in identifying wake regions near the inlet and outlet, but also in quantifying potential in future aero dynamical improvements.

The geometry improvement consisted of moving the compressor component in the hope to reduce pressure losses close to the inlet of the heat pump, and also to achieve a more even distribution of flow for the condenser but the results that showed the compressor placement had no relevance to either conditions.

Abstract (Swedish)

Att torka kläder är en nödvändig men energikrävande process i det moderna samhället. Ett vanligt sätt att torka kläder är med torktumlare. Electrolux är en världsledande leverantör av hushållsmaskiner och för närvarande utvecklar de en ny modell av en värmepumpstorktumlare. Det här examensarbetet studerar de aerodynamiska egenskaperna i det interna luftflödet för nämnda torktumlare. Om tryckförluster i systemet kan reduceras så kan energin som driver fläkten reduceras. Målet är att identifiera tryckfördelningen och potentiella geometriförbättringar över systemet. Arbetet har bestått av att bygga en prototyp för en teoretisk modell av tryckfördelningen, CFD simuleringar av värmepumpssidan av geometrin, samt test av en idé till geometriförbättring testades i CFD och mättes i labbet i Ljungby.

Den teoretiska modellen byggdes med mängd tvätt och filter som input och tryckfördelning som outputs. Modellen var användbar för att identifiera kritiska kombinationer av last-fall och filtertäppningsgrad där undertryck bibehölls i trumman, vilket är hjälpsamt för att hålla gummiförseglingarna täta.

CFD-simuleringar genomfördes på luftflödet för värmepumpsdelen av geometrin. Resultat från detta var användbart för att identifiera regioner med recirkulationsbubblor nära inloppet och utloppet, men också för att kvantifiera möjligheterna för framtida aerodynamiska förbättringar.

Geometriförbättringen bestod av att flytta kompressorn i värmepumpen ut från luftflödet, detta i förhoppningen att reducera tryckförluster nära inloppet samt att få en jämnare hastighetsfördelning vid kondensorn. Resultaten visade att kompressorn inte hade någon signifikant effekt på något av de undersökta förhållandena.

Preface

The research for this thesis has been made between January-December 2017. The work has been made at Lund University (LTH) and at Electrolux Laundry Systems department in Ljungby. The goal of the research has been to increase the understanding of pressure loss distribution and to find aerodynamic improvement potential in a new heat pump dryer, but also to develop and valuate such methods so that the knowledge of these studies can be applied on other laundry systems in the future. A special thanks to Robert Zoltan Szasz at LTH energy department and to Mattias Johannson, and Mikael Blomqvist from Electrolux professional for their relentless mentorship and guidance. Thanks to the remaining staff at Electrolux professional Ljungby for a general welcoming and helpful spirit.

Contents

Nomenclature

P	**static pressure (Pa)**
Q	**volume flow (m^3/s)**
k	**pressure loss parameter [kg/m^7]**
K	**normalized pressure loss parameter**
a, b	**generic variables**
FC	**filter clog (%)**
load	**load (kg)**
LF	**load factor**
evap	**evaporator**
cond	**condenser**

Acronyms

CFD	**computational fluid dynamics**
HEX	**heat exchanger**

1 Introduction

Drying clothes is an important process but in modern days it's also an energy demanding one, both on industry and household levels. To reduce energy usage it is important to get as much hot and dry air in contact with the fabric as possible while still maintaining a required time efficiency for the drying cycle. The technical development of tumble dryers has led to a couple of different configurations in how the airflow is directed. The most common application is the fully axial fan solution where air is sucked in through one end of the machine and exits through another. This leads to a lot of excess heat being lost in the exit air. With a heat pump dryer the air is in a theoretically closed cycle, which lowers the lost energy. The goal of such an application is to increase the effect and capacity of the dryer machines to compete with other brands. The lowered energy requirements will lead to lower costs per cycle for the user and the increased capacity will make the application more time efficient.

Electrolux is one of the world leading manufacturer and developer of household appliances. Every day their research groups are working to make Electrolux machines even more competitive on the market. One of their current projects is a closed cycle heat pump dryer. This thesis will be entirely based on that new prototype.

Goals for the thesis are:

1. Investigate the potential in making a theoretical model of the pressure losses in the heat pump system. How can such a task be solved methodically and can that process be automated/generalized and to what degree?
2. To investigate the heat pump side of the dryer using CFD-methods. This will give more complete overview of how the air flow behaves inside the machine, which is hard to quantify using only lab results.
3. Lastly, the data from the CFD simulations will then be used to make at least one improvement suggestion to the geometry. Reducing pressure losses in the cycle might mean that less energy will be required for the fan, thereby making the machine more energy competitive, both in an environmental and economic sense. Other potential optimizations that could be made would be a more even flow distribution over the heat exchangers to make them work more efficiently.

The entire CFD-part of the study will be calibrated and compared to lab measurements, collected at the Electrolux laboratory in Ljungby.

1.1 Literature study

As a first part of this thesis, results from previous studies in similar subjects were collected.

1.1.1 Energy conservation potential in tumble drying

In a study of hybrid heat pump clothes dryers [1] some economic and energy aspects of clothes drying in the US are discussed. 4% of residential building electricity consumption are from tumble dryers, and the amount of units are predicted to increase from 92.5 million units to 105.8 million units between 2015 and 2025. In addition it's stated that dryers contribute to high household peak loads, putting local power distribution transformers at an increased risk of overloading.

In a review of global energy consumption [2] it is found that households contribute to 27% of energy consumption and 17% of carbon emissions. The residential CO2 emissions has grown by 2% during the last two decades. Electrolux's core market is in Western Europe, North America Australia, New Zealand and Japan. The top 10 emission countries contains Canada, US and Japan which are all deemed to have a substantial part of their energy consumption in their residential sector.

1.1.2 Systems of tumble drying

There are currently three technological designs to define a tumble dryer system [3]. These are the open-loop, closed-loop and a midway solution called partial recirculation design. The open-loop system is where ambient air enters through a heater, passes the drum and ejects wet cold air into the surrounding. Such a system has the disadvantage of lint and wasted heat getting ejected in the exhaust. The closed-loop system is the one used in the prototype being investigated in this thesis. The closed loop has the theoretical advantage of not wasting as much heat energy and trapping more lint, but the solution has some design challenges. One of these challenges is and increased drying time [3]. The partial recirculation solution uses some of the exhaust air but not all, leading to the lint issue from the open-loop remaining and some of the heat energy being lost, but provides a more stable solution.

1.1.3 Theoretical model

To make a model of the system behaviour for different load cases, it is essential to have a fan performance curve and to model the system load curve as described in a performance study of centrifugal fans [4]. The fan curve is predetermined and accessible from the manufacturer of the fan and is commonly of the type:

$$P_{fan} = P_0 - k_{fan} Q^2 \qquad (1)$$

The system load curve is specific for each load case as eq.2 where k is dependent on the load case.

$$P_{load} = k_{load} Q^2 \qquad (2)$$

By identifying the point where the fan curve and the system load curve pressure intersects such as $P_{fan}=P_{load}$, for that particular load case and fan the values of P and Q can be found.

A wind tunnel study was performed in Mondragon University [5]. In that study pressure losses were of main interest, similar to this thesis. In the wind tunnel model the system is divided into sections dependent on the shape of the geometry. As many of the sections are cylindrical or semi-cone shaped, the section losses can be estimated using predetermined functions. The variables used for section losses are length, hydraulic diameter and friction factor. All these variables are joined together to form the normalized section loss parameter K. K varies mainly dependant on the general

geometrical shape of the section. In the end the total pressure loss for the system is expressed as a sum of the section pressure losses.

$$\Delta P = \sum k_{section} Q^2_{section} \quad (3)$$

A similar approach is feasible in this thesis for building the theoretical model. However the shape of the geometry sections in the heat pump dryer are much more irregular shaped compared to the wind tunnel. The function for the pressure loss parameter will be based on experimental data for load cases instead of predefined functions based on length, friction factors and hydraulic diameters.

The wind tunnel study then proceeds with the researchers making a CFD model of the case and comparing differences of the pressure loss estimation for CFD and the theoretical model. It is found that their theoretical model was lacking when estimating secondary losses (which are based on cross sectional change).

1.1.4 CFD part

A study made at Karlstad University investigates potential geometry improvements for a tumble dryer based on CFD methods [6]. The study is more focused at the side with drum, hatch and filter. The boundary is set from the exit of the drum, through the filter and ends at the inlet to the evaporator. The suggestions for improving the geometry is smoothing out 2 sharp edges in hope to reduce vortex effects. An interesting approximation made in the study is the modelling of the filter, where porous media is used with a porosity (amount of open area) of 43%.

The reduced sharpness leads to pressure drop reduction of roughly 3% and 23% for the 2 modifications inside the defined boundary. The study does not only limit itself to pressure drop, but flow uniformity is also investigated, and the modifications improve uniformity at the outflow by 3%. As a final conclusion it is stated that modelling of the entire tumble dryer domain would be of interest but was not achievable because computational and time constraints. Modelling of the fan, drum and heat exchangers would be challenging. To model such components it is suggested to analyse them separately prior to simulation.

A study from Tsinghua University Beijing [7] investigates a porous media approach to CFD simulation of a heat exchanger. The heat exchanger is of a shell and tube type and is applied in a sodium cooled fast reactor. The study states that modelling all the tubes for the Heat exchanger is not feasible and that a porous media is sufficient both for the heat exchange and for the pressure loss. The porous media is stated to not greatly affect the accuracy of the simulation. To design the porous media, pressure drop is correlated to experimental data. As the study continues it focuses on how accurately the model can predict heat exchange and flow uniformity. When comparing the experiments with the simulation results the temperature deviated less than 5% which was deemed successful.

The method of using porous medium seems suitable to this thesis case and it is of interest to note how the porous media is calibrated using experiments.

1.2 Overview of the geometry

This is an overview of the tumble dryer from Electrolux. The entire air flow geometry is relevant for the theoretical model, but only the heat pump side of the air flow geometry is part of the CFD study.

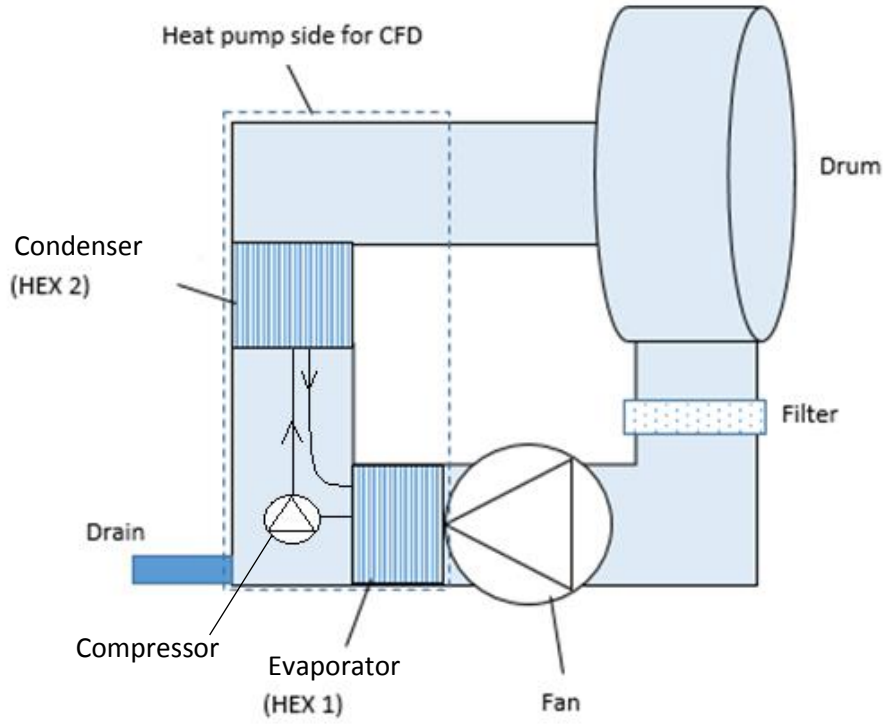

Figure 1 The Electrolux closed cycle tumble dryer system

The tumbler design works as follows: Cold wet clothes are put in the drum. The drum spins which helps to maximise the contact between the air and the wet surfaces. The fan sucks moist air through the filter (which separates lint by-products from the clothes) and launches the air through the heat pump part of the systems. The two heat exchangers are part of a separate closed system with compressor, choking valve, the two heat exchangers and refrigerant fluid. The water in the moist air is condensed at the evaporator and water is extracted through the drain. As air exits the heat pump system it is hot dry air that goes back into the drum.

2 Method

2.1 Scope of study

The main tasks in this master thesis can be summarized as follows:

1. To make a system model, first the system case has to be analysed to identify important components, variables and system borders. Limitations and simplifications will be made to make it reasonable to build a prototype of a theoretical system model using Matlab. When the simplified case has been established, previous lab results and component specifications will be used to establish how much every component contributes to the total pressure load for variable inputs. A theoretical model will be constructed to approximate flow and pressure based on the known lab-data. The implication and usefulness of this model will then be discussed.
2. A CFD model will be constructed to analyse the heat pump side of the geometry (see figure 1). This will be based on CAD-files and drawings from Electrolux. Simplifications will be made to not include too many components and complicated small geometries. This is to make the simulations more stable and reasonable. To validate the realism of the results, further measurements will be made on the actual machine at the Electrolux laboratory in Ljungby. The model will have input data decided based on results from the system-model.
3. Based on observations in the system model and the first simulations, a suggestion to improve the geometry will be provided and investigated. The potential gains of this will be compared to the system in its entirety to decide if any change has enough impact to make it relevant.

2.2 Detailed method

2.2.1 System model

As the initial system is investigated, 5 main components in the air flow are identified: the fan, evaporator, condenser, drum and filter. Between all of these components are potential leakages of air to various degrees, especially close to the drum as all the moving components make it difficult to get an entirely air tight environment. The drum has more leakage if the gauge pressure is positive as the rubber sealing for the hatch is tighter if there is suction on that part of the system.

The load cases vary from an empty drum to 20 kg of dry clothes. It is also noted that the filter clogs up over time with lint from the clothes. Users of the tumble dryer sometimes ignore to clean the removable filter and that can lead to a highly increased load, as the clogged up filter makes it harder to suck the air through the system. The air moisture and total amount of water in the system varies over a cycle, as a drying cycle begins with wet clothes. The water is evaporated over time, then condensed in the heat pump part and extracted in liquid form via a pump. As the clothes are dried, the amount of total water and moisture decreases.

The temperature is also varying through a normal cycle. It starts with cold wet clothes that are heated up. As the evaporating water has a cooling effect, when the clothes become nearly dry the temperature goes up drastically at the end of the cycle.

As the main purpose of this study is to investigate aero dynamical improvements to the geometry, the system model for this study will assume dry air with a constant inlet temperature of 0˚C at 100000Pa. These values were chosen for pressure and temperature because all lab data in Electrolux for the dryers are recalculated and normalized to those values. Load cases of 0-20kg of dry clothes with 0-90% clogged filter will be investigated, making those two variables the input for the

theoretical model. The filter clogging is assumed to be evenly distributed. Variation in temperature and moisture will be ignored for simplicity's sake. Figure 2 shows the initial system model and the model after simplification. The evaporator and condenser are adding in the study an aerodynamic resistance, but are assumed to have no heat exchange in the model.

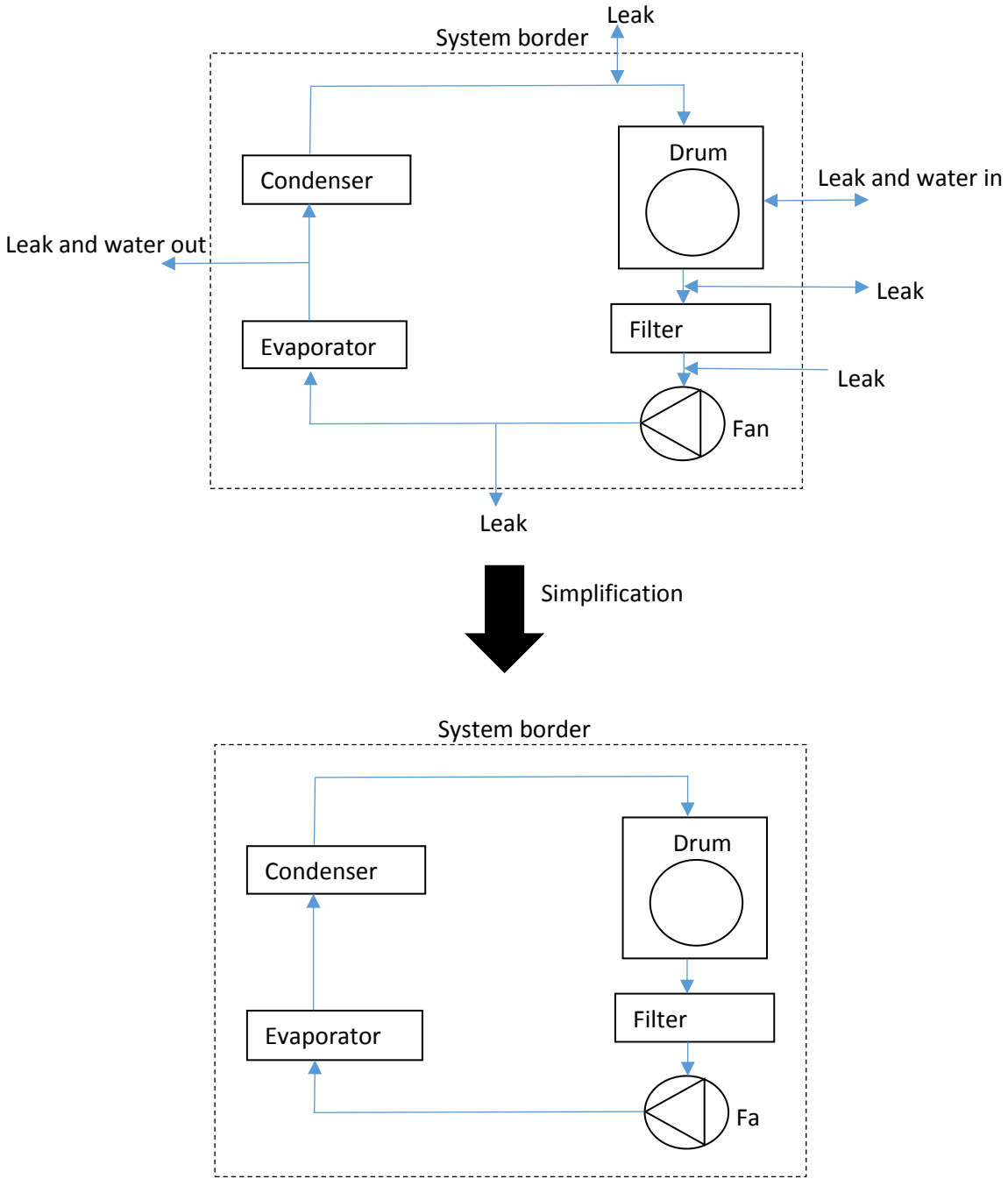

Figure 2 The system as defined and simplified for this thesis.

As the scope of the theoretical model had been decided, it was time to get a more intricate picture of how the components interact. Previously measured lab data from Electrolux was gathered. That data contained volume flow measured between the fan and the evaporator, and between the condenser and the drum. The volume flow had been measured using Venturi meters. Static pressure had been measured between the fan and the evaporator, between the evaporator and condenser, between the condenser and the drum, between drum and filter and between filter and fan, all using Pitot static tubes.

Using a manual iterative method and mathematical function knowledge, a general model was written in Matlab as a function based lab data for relevant load cases and degrees of filter clogging. This model describes the pressure loss in different components throughout the system.

To write that model, first the overall fan performance curve and system load curve was decided. They are constructed as suggested in the literature study using eq.1 and eq.2. When fan performance curve and system load curve intersects they describe the volume flow and pressure loss for the entire system at that load condition.
As the resistance for the flow is provided by different components, eq.4 can be assumed (similar to eq.3 in the literature study chapter 1.1.3). To make the assumption that the load can be divided into segments like eq.4 it has to be assumed that Q remains constant throughout the geometry (no leakages).

$$k_{load} = k_{evaporator} + k_{condenser} + k_{drum} + k_{filter} + k_{remaining\_geometry} \quad (4)$$

Equation 4 is then simplified in the model to include the remaining geometry resistance in the nearby components. For example the empty ducts near the filter are assumed to be a part of the filter.

$$k_{load} = k_{evaporator} + k_{condenser} + k_{drum} + k_{filter} \quad (5)$$

To write the Matlab function these pressure loss parameters *k* for the load cases are the variables that have to be described for each component. Their inputs will be load (kg) and filter clogging (%) like in eq.6.

$$k_{load} = F_1(load, FC) \quad (6)$$

The gauge pressure is of interest, because of the behaviour of leakage in the drum. When the pressure is less than the ambient pressure in the drum, suction is created and the rubber seal works well. If the drum has more pressure than the ambient air, the leakage increases from the drum and the performance decreases. If there was no leakage in the circuit, then the pressure immediately before and after the fan would be as eq. 7 and 8 and $P_{average}=P_{ambient}$ would be true.

$$P_{before\_fan} = P_{average} - \frac{P_{load}}{2} \quad (7)$$

$$P_{after\_fan} = P_{average} + \frac{P_{load}}{2} \quad (8)$$

However if a leakage is introduced an interesting occurrence happens. If the leakage is placed in a point with positive gauge pressure, this pushes out some of the air in the circuit. This happens until a pressure balance is achieved for the leaks and leaving the average pressure in the circuit lower than $P_{ambient}$. If the leakage is close to the negative gauge pressure side instead, the opposite would happen and the circuit overall pressure would increase to reach a stable pressure balance.

The load distribution of the components shifts where the 0 point of gauge pressure is and therefore affects if $P_{average}$ becomes higher or lower than $P_{ambient}$. This means $P_{average}$ will have to be described as a function of load and filter clog.

All the variables of interest have been identified and the formulas needed for the complete system model are given in eq. 9-14

$$k_{load} = F_1(load, FC) \quad (9)$$

$$k_{evaporator} = F_2(load, FC) \quad (10)$$

$$k_{condenser} = F_3(load, FC) \quad (11)$$

$$k_{drum} = F_4(load, FC) \quad (12)$$

$$k_{filter} = F_5(load, FC) \quad (13)$$

$$P_{average} = F_6(load, FC) \quad (14)$$

Assuming these functions could be modelled, the pressure could be plotted along the components of the system as in figure 3:

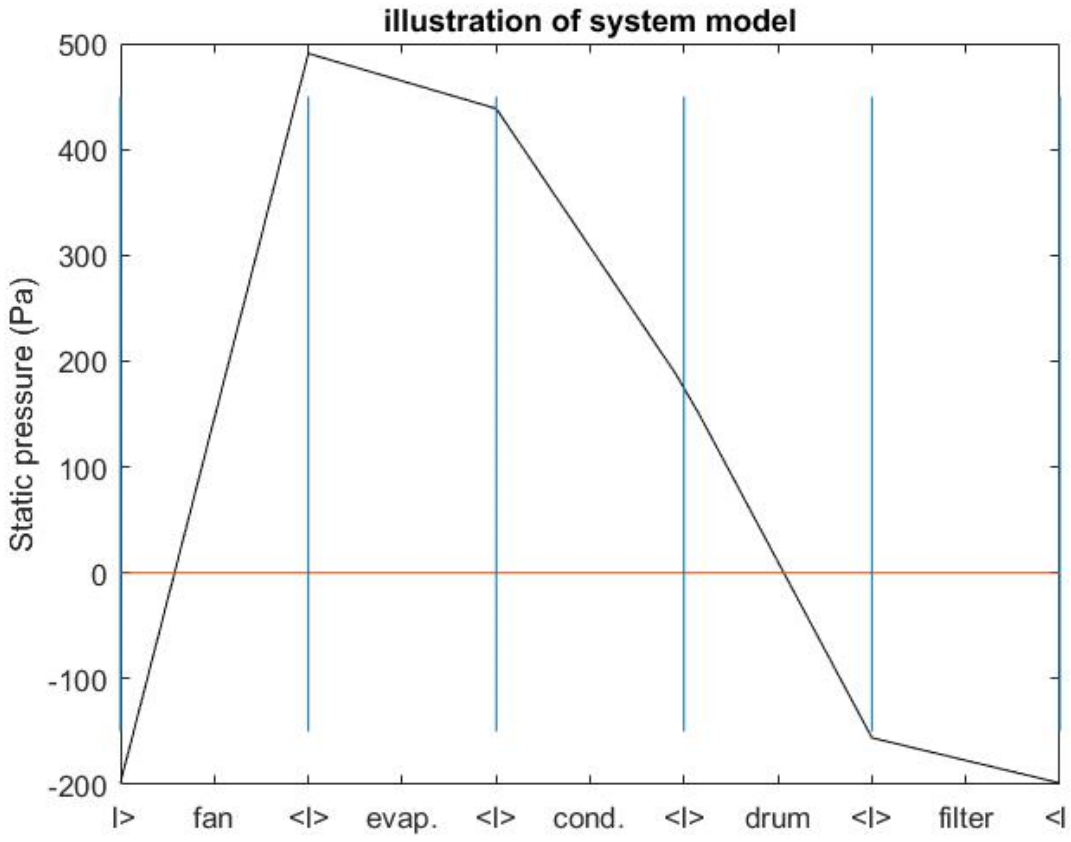

Figure 3 Illustration of how the pressure could be plotted along the components. evap. =evaporator, cond. =condenser. I> indicates start of components. <I is exit of component. For example I> fan <I is the entire fan geometry with low pressure at entry point and high pressure at exit point.

The pressure at the entry of the fan would be $P_{average}$-P_{load}/2. For the evaporator entry the pressure would be $P_{average}$+P_{load}/2. To get the pressure at condenser entry the solution would be $P_{average}$+P_{load}/2-$k_{evap}Q^2$. Eventually after going through all the components we have returned to the fan entry and the same pressure as when we started. Of note is that the entire curve in figure 3 would look different for each input of load and filter clogging. In the example given $P_{average}$ is roughly 200Pa. If there was no leakages $P_{average}$ would be reduced to 0Pa and the entire drum would have negative gauge pressure, which would make the rubber seal on the hatch perform better.

2.2.2. CFD simulation

With the system model complete the work on the CFD simulation could start. The case was made in 3D. A CAD file of the heat pump side was provided by Electrolux. This was cleaned from all excess components like screws and pipes. Such intricate details would make the simulation require a finer mesh, more advanced turbulence models and more simulation time, while not being necessary to get an idea of the geometry's overall aerodynamic properties. All holes in the Cad file were sealed until all that's left was the shell of the geometry where the air would flow. To increase the stability of the solution the outlet is extended by 0.9m and narrowed with roughly 15˚ angle in the exit of this extension. This is to avoid any backflow in the outlet as that can disturb the reliability of the boundary conditions. Any pressure losses in this extension will be discarded for the result. The mesh type of tetra/mixed is chosen to help in the mesh to adapt to the irregular nature of the geometry. The mesh has a hexa-core to reduce unnecessary complexity and number of elements at the core of the geometry. Hexa-meshes are usually leading to better accuracy and stability. The finished mesh is illustrated in figure 4.

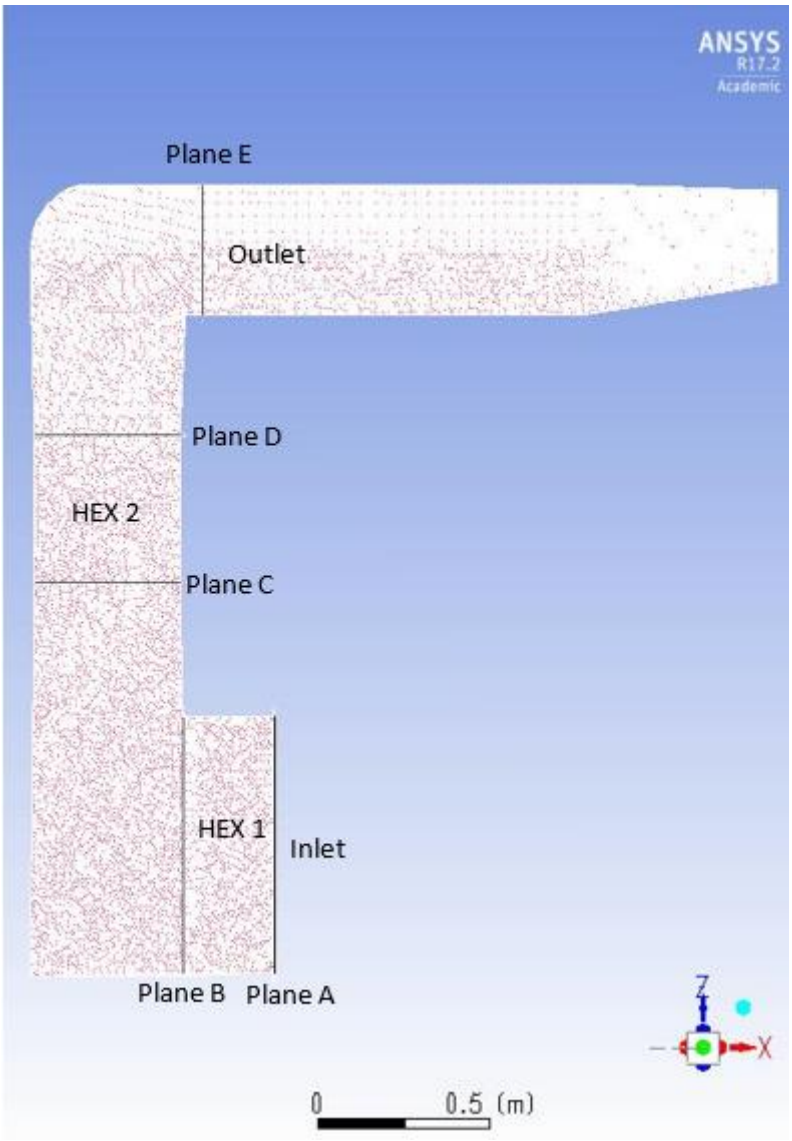

Figure 4 The mesh For the Heat pump-side airflow geometry. Noted the added extension after the outlet that increases solution stability. The parts corresponds to the heat pump side defined earlier in figure one.

5 planes (A, B, C, D, and E) were defined at the boundaries to the heat exchangers and the heat pump geometry for post processing purposes.

It is important to choose a cell resolution suitable for the case. A too fine mesh will take too long to calculate, and at a certain level of resolution the results barely change as the simulation hopefully has reached a case which is close to reality. A too coarse mesh will not be a good representation of the real flow, and therefore less useful. To help select the right size of the mesh, a mesh study for a couple of mesh sizes is performed. This mesh study will indicate the accuracy of the simulation results. The meshes are of the same type but different sizing, leading to increasing node numbers for the finer meshes. See table 1.

Table 1 Amount of nodes for the different meshes made to test grid independence

Mesh	Mesh 1	Mesh 2	Mesh 3	Mesh 4	Mesh 5	Mesh 6	Mesh 7	Mesh 8	Mesh 9
nodes	44k	92k	173k	283k	537k	1,2M	1,3M	2,0M	3,9M

Two load cases are investigated. These will be 0kg load 0% filter clog, and 20kg load 90% clogged filter. The difference between these two cases will effectively only be the air speed at the inlet to the heat pump side. Using the data for the measured volume flow, the known inlet area, surrounding absolute pressure of 100000Pa and temperature of 0˚C the inlet velocity becomes 2m/s and 1,2m/s respectively. For general settings a pressure based solver is used as this is a low speed flow and density changes should be small throughout the flow. A steady solution is sought as instantaneous profiles are of no relevance. However, if the case would have included the temperature changes and humidity changes over time as a full laundry cycle would do, a transient time based solution would have been useful. Absolute velocity formulation was chosen.

The equations solved by Fluent are mass conservation and momentum conservation equations. The energy equations are not needed because there is no heat transfer in the model. To account for turbulence, a standard k-epsilon model is used with enhanced wall treatment. K-epsilon approximates turbulence by modelling turbulent kinetic energy and turbulence dissipation rate. A quick run of K-w SST model was also run on the final mesh to check model dependency, and a difference of inlet pressure 0.56% was found compared to the k-epsilon solution. All equations used are further described in the Ansys user manual [9].

The material chosen for fluid is air, with density recalculated for 100kPa and 0˚C. The density for those conditions is 1.276 kg/m^3 and the viscosity 1.719e-5 Ns/m^2 [8]. As viscous effects are of importance for the study, the walls are set as no-slip.

The solution method used the SIMPLE scheme. The gradient was selected to be least square cell based. Standard pressure scheme was used. The momentum, turbulent kinetic energy and turbulence dissipation rate were set to first order. To receive an even better solution second order schemes could have been used to refine the cases further. This was not done because of time constraints.

2.2.3 Lab data to calibrate the CFD simulation

The lab-rig used to collect data for use in the CFD-model, was the same rig previously used by Electrolux for the measurements used in the theoretical model (chapter 2.2.1), but with some modifications. The volume flow was measured using Venturi meters before plane A and after plane E as previous measurements. The volume flow was regulated to get data corresponding to the two desired load cases as defined in 2.2.1. Static pressure was measured using Pitot static tubes centrally placed at Plane A, C and E. These measurements would be used to calibrate the correct resistance for the heat exchangers.

The measurement instruments collected data once every second. The volume flow measurements 1h data with output value at every 1 second. The volume flow was measured for this long because it was running during all the other measurements. The static pressure measurements was each made for 300 seconds with output at every 1 second.

To regulate the volume flow a plate is used to cover the filter partially until the sought air flow velocity (2m/s and 1,2m/s for the two cases) was achieved.

2.2.4 Lab data to validate the CFD compared to real geometry.

The idea was to compare velocity profiles from the finished CFD results with some locally measured velocity values. This would theoretically be a way to validate how realistic the simulation results are. However the only available instrument to make such a measurement was pitot static tubes which are not optimal at low velocities. So it remains to be seen if such a method could be useful in validating the CFD simulations.

Velocity in the x-direction in plane E and velocity in the z-direction in plane C was measured using Pitot static tubes along 4 traverses built using metal rods. The Pitot static tubes had output for static and dynamic pressure. Both of these were connected with hoses to a digital instrument. Both output pressures had to be zero calibrated manually for the digital instrument. Since the difference in static and dynamic pressure is quite small for low air velocity it was important to get this zero calibration perfect. The metal rod traverses was there to fixate the pitot static tubes in the flow direction. The metal traverses were placed centrally along the z- and x-axis for the plane E and along the x- and y-axis for plane C. 5 equal distance points along the profiles were measured along all traverses except for plane C, x-direction which because of space limitations only measured 3 points. These measurements will be compared to plotted velocity profiles from the CFD results to compare if the air flow distributes differently in the actual lab rig and the CFD simulation, which could indicate if the simulation results are realistic.

Each point for the velocity along traverse measurements was made for 300 seconds with output value at every 1 second. To regulate the volume flow a plate is used to cover the filter partially until the sought air flow velocity (2m/s and 1,2m/s for the two cases) was achieved.

2.2.5 Modelling of heat exchangers

A challenge of the project was to find a suitable model for heat exchangers. As suggested for similar geometries in previous projects [5], [6], the porous medium method was used. Based on lab results the pressure before and after the heat exchangers for high and low load cases was known. The high velocity (low load) case data was used as value to calibrate the resistance in the porous medium, and the simulation results were then compared to the low velocity case to validate how good the porous model adapts. The resistance of the porous zones are tested by iterations until they gave results that correspond to the low load lab case. This would mean a guessed value was selected for resistance, initially for one of the simpler test mesh. The value was readjusted until results was acceptable. As a finer mesh was selected the resistance had to be fine-tuned. The design in the heat exchangers was so that lots of thin walls were parallel. Therefore the flow could not move in y-direction, the resistance was set at least 100 times higher in y-direction to capture that effect. There was 2 options to set resistance in the porous medium, “Relative velocity Resistance Formulation” or a constant resistance. Relative velocity Resistance Formulation was chosen to make it more realistic for varying volume flows.

Table 2 velocity resistance in the porous medium (1/m^2)

	hex1
x-direction	6000000
y-direction	2,00E+10
z-direction	6000000

	hex2
x-direction	2,20E+07
y-direction	9,00E+10
z-direction	2,20E+07

2.3 Suggestion to improve the flow

As the lab measurements were being made, it was observed that the compressor was placed in the flow path. As no one had previously investigated the effects of this component on the air flow, a decision to investigate the effects of this components placement was made. Two effects of relevance were to be investigated.

- Does the compressor's placement increase overall pressure loss in the system significantly?
- Does the compressor change the flow distribution at the inlet to HEX 2, thereby making it less efficient?

To investigate this, a new case has been set up where the compressor is modelled by the addition of two cylinders. The mesh was generated in the same way as the compressor free case and it was run with the same boundary conditions. (See figure 5) The compressor case will be compared directly to the standard case.

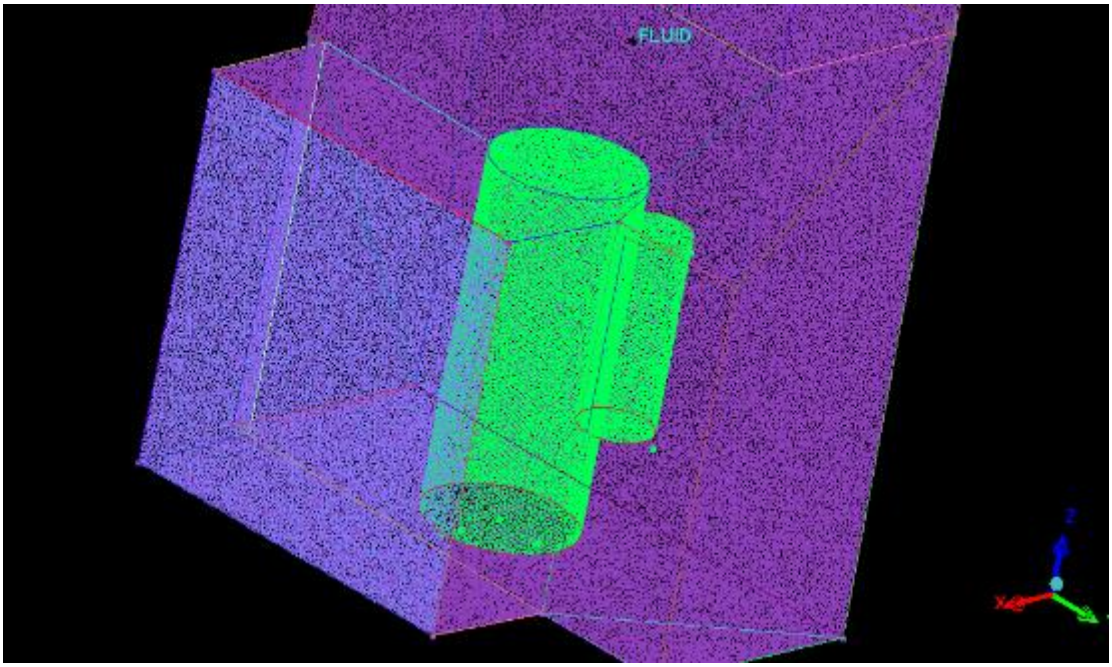

Figure 5 Compressor modelled in the mesh.

3 Results and discussion:

3.1 Matlab theoretical model of flow

As described in the literature study and the method, the fan performance curve and the system load curve are essential together to describe the pressure and volume flow for each different load case. In the following figure, some generic load cases with made up values for k are plotted in green for illustrative purposes. The pre-given and approximated fan performance curves are in red and yellow.

3.1.1 Fan curve and system load curve

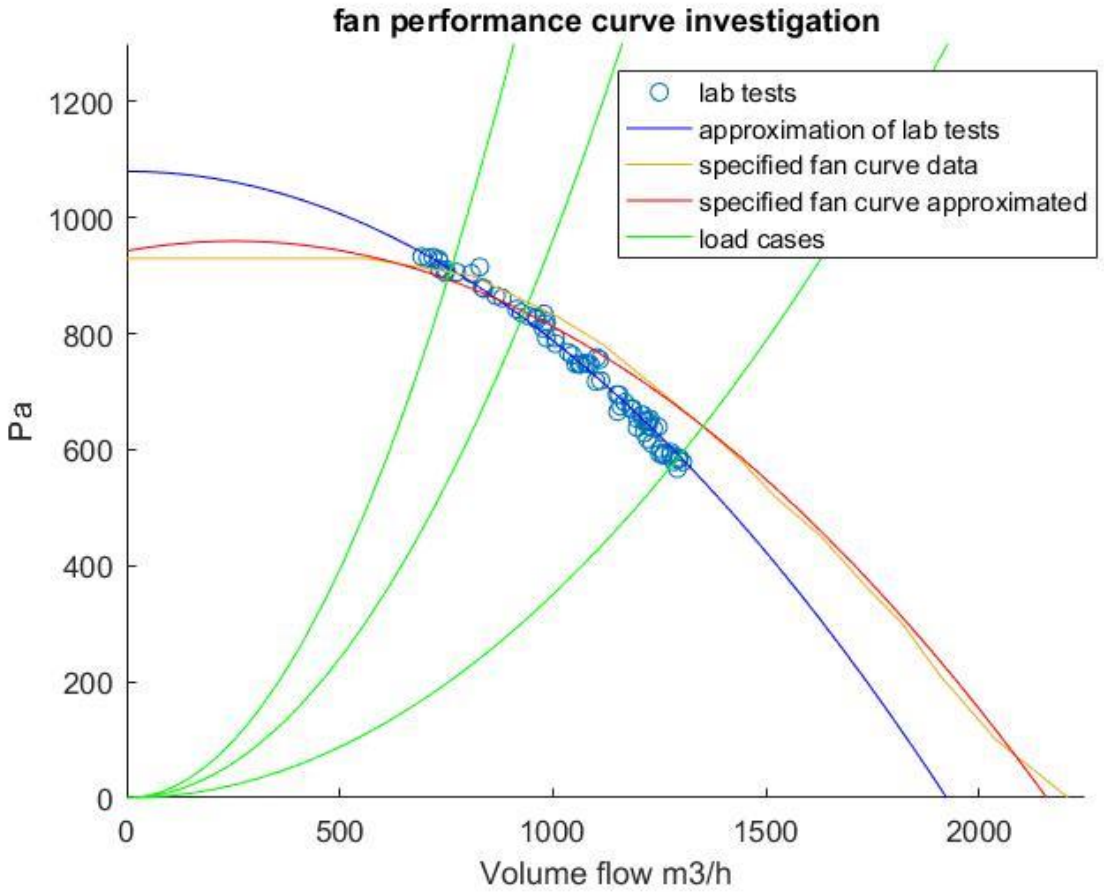

Figure 6 Measured fan curve (blue) and some example load case curves (green). Predefined fan curve (blue and yellow). The pressure on y-axis is the overall pressure rise from the fan and also corresponds to losses of pressure throughout the system for the system loss curves.

The pre-specified fan curve (figure 6, red and yellow) did not match the lab results. The reason for that are probably slight differences in measurement conditions at the manufacturer and in the Electrolux laboratory. A decision was made to adapt a new fan curve (figure 7, blue) and use this new adapted equation for the final model. That decision means that the theoretical model will correspond more to lab results at Electrolux than predefined component specifications. The adapted function based on the lab results was eq.15-16.

$$k_{fan} = -1.05 \cdot 3600 \quad (15)$$

$$P_{fan} = -1.05 \cdot 3600 \cdot Q^2 + 1080 \quad (16)$$

This estimation means the model will only be viable for flow cases of 600-1300 m^3/h, which corresponds to the lab data and the relevant load cases. (0kg laundry & clean filter to 20kg laundry 90% clogged filter).

3.1.2 Finding $P_{average}$

Plotting $P_{average}$ from lab data based on filter clogging and load case gives figure 7. There were two measurement points to get these values. One before inlet to HEX1 and one after the filter (see figure 1 for clarity). These points make up the lowest and the highest points of pressure in the system due to the points being the closest to the fan. The average value for pressure of these two points are the sought after average gauge pressure (see figure 3 for an overview).
Two similar measurements were made where the only difference was a porous plate at the inlet to HEX1. The plate had such large holes that it had no significant impact on the overall pressure. To get a more statistical weight to the measurements, the measurements both with and without the porous plate were added to the data series. It can be observed in figure 7 that every point has two values close to each other because of this.

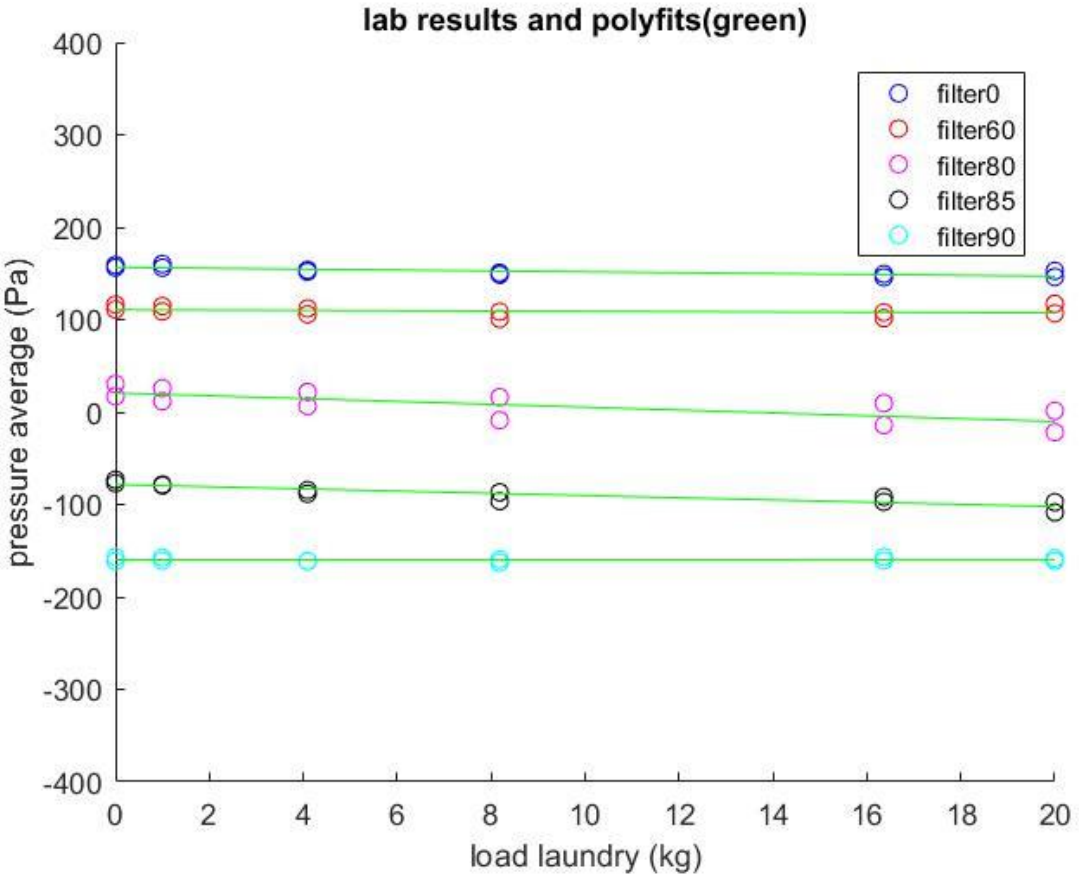

Figure 7-pressure average for various filter clogging (%) and load cases

After observing figure 6 it was decided that $P_{average}$ can be modelled as a linear function as equation 17. The load factor (LF) is introduced to make sure the equation has the correct units. LF is related to the amount of load and it varies from 0-20, since the load varies from 0-20kg.

$$P_{average}(FC) = P_{initial}(FC) + P_{variable}(FC) \cdot (LF) \qquad (17)$$

The components for this function are investigated separately to determine $P_{initial}$ and $P_{variable}$.

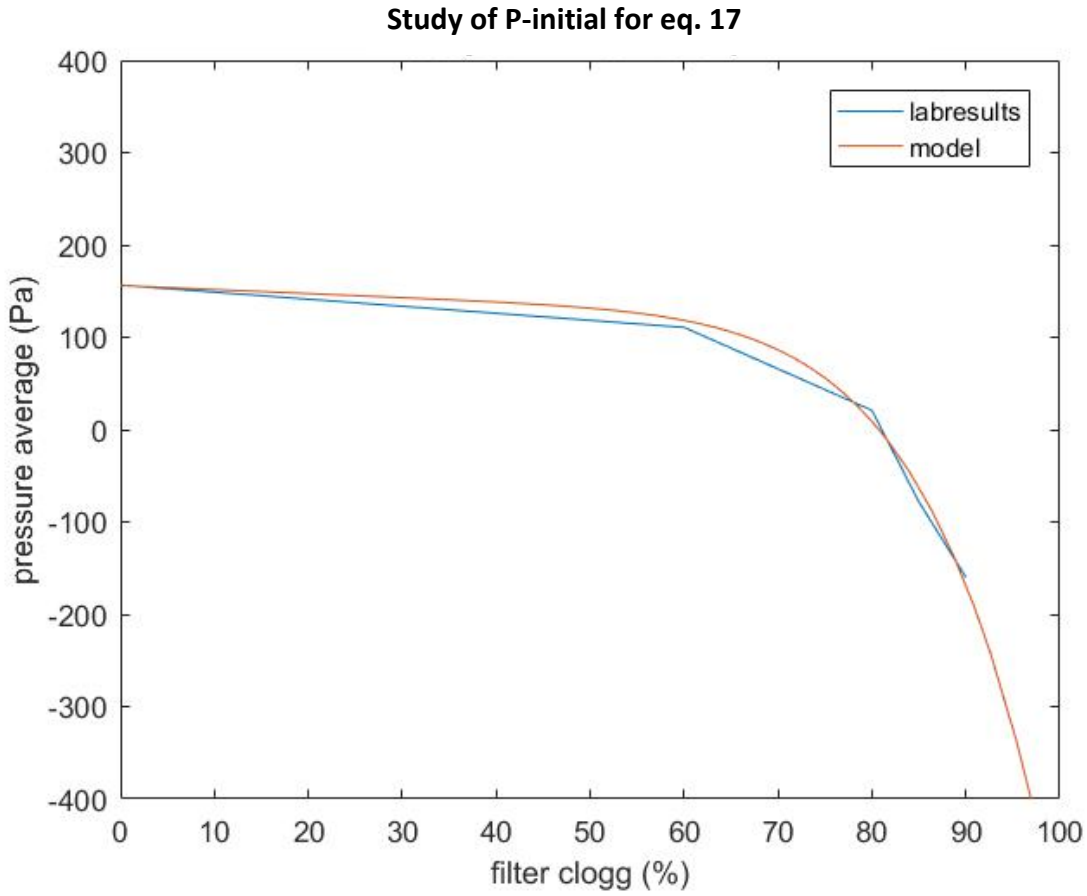

Figure 8 Experimentally measured $P_{initial}$ from eq. 17 and the curve-fit used in the model.

The experimentally measured $P_{initial}$ values are shown in figure 8 (blue). In order to model the variation of $P_{initial}$ exponential function has been fitted to match the experimental data. The resultant curve is given by eq.18 and is shown with a red line also in figure 8. The level of accuracy is deemed to be sufficient

$$P_{initial} = 156 - (FC/44)^{7.9} - \frac{FC}{2.3} \qquad (18)$$

To determine the other unknown function ($P_{variable}$) that makes up the second part of eq.17 a similar strategy has been adapted. The experimental data and model for $P_{variable}$ are shown in Figure 9.

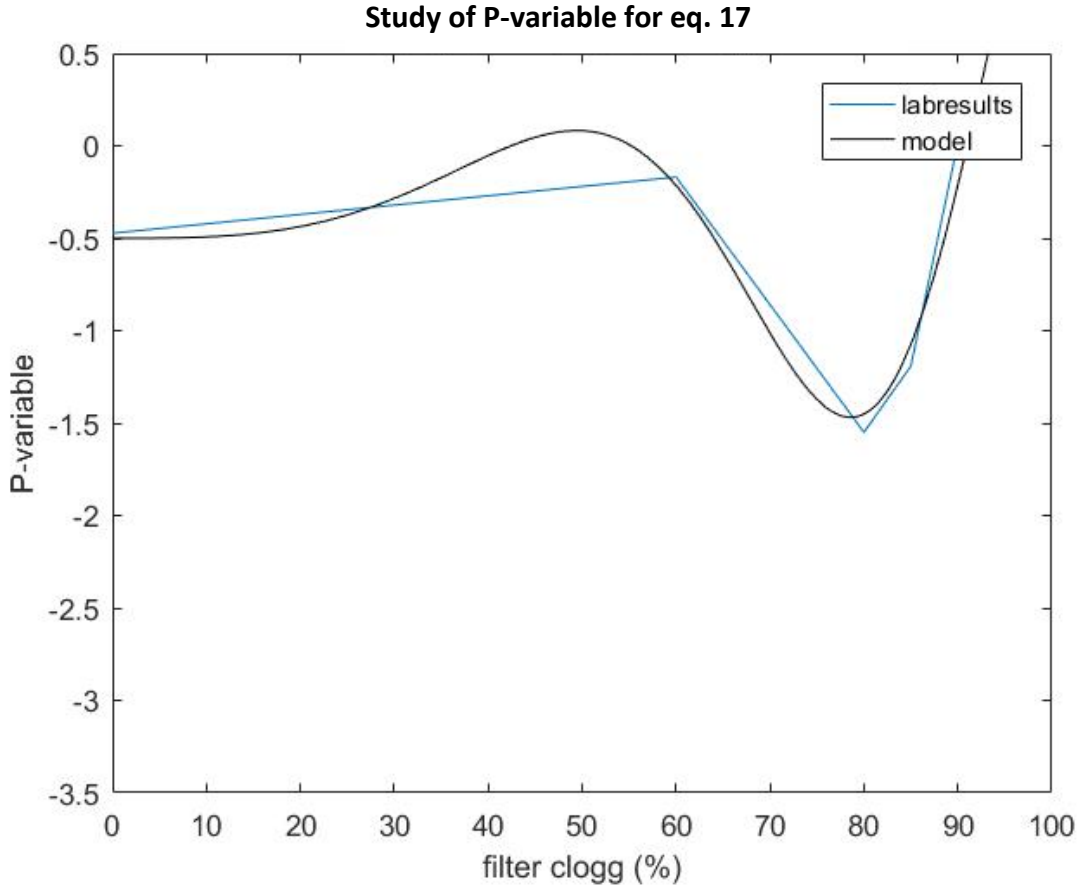

Figure 9, continuation of solving eq.17. This is for the $P_{variable}$ part.

To match the oscillating nature of the function a sinus curve part is used. To catch the growing nature of the curve an exponential part is also added, which is designed to only have an impact on high filter clogging. The result is equation 19

$$\mathrm{P_{variable}}(\mathrm{FC}) = \sin\left(\frac{\mathrm{FC}^2}{1300}\right)\cdot\frac{\mathrm{FC}^{1.19}}{170} + (\mathrm{FC}/100)^{10} - 0.5 \qquad (19)$$

Together equations 18 and 19 form the sought model for $P_{average}$ and completes equation 17.

3.1.3 Finding k_{load} to access modelling of Q and P_{fan}

k_{load} was investigated and found in a similar manner to $P_{average}$. To get k_{load}, equation 2 and 16 together with $P_{fan}=P_{load}$ was rewritten as eq. 20.

$$\begin{cases} P_{fan} = -1.05 \cdot 3600 \cdot Q^2 + 1080 \\ P_{load} = k_{load} Q^2 \end{cases} \Rightarrow k_{load} = \frac{-1.05 \cdot 3600 \cdot Q^2 + 1080}{Q^2} \quad (20)$$

The lab result recalculated into the form of eq.20 was then plotted in figure 11.

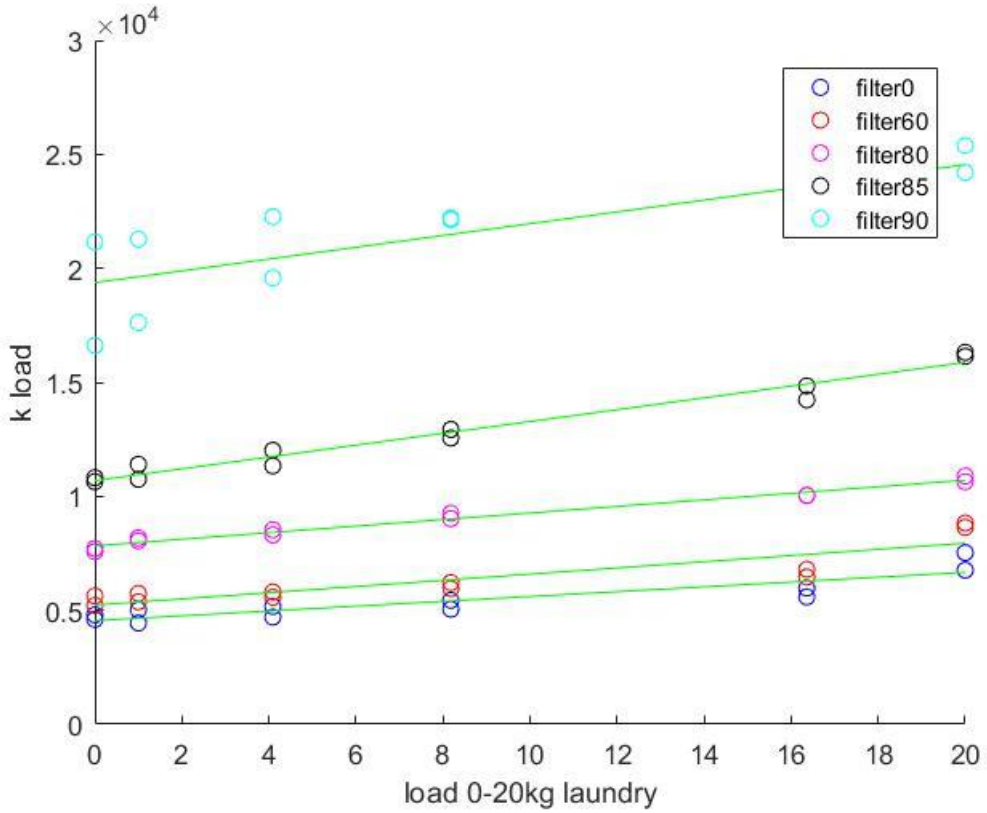

Figure 10 k_{load} plotted as a function of filter clogging (%) and load (kg)

k_{load} was plotted for different load and filter points according to lab data and just like in the study to find $P_{average}$. It was found that a similar linear function could be estimated for figure 10 in equation 21.

$$k_{load}(FC) = a(FC) + b(FC) \cdot (LF) \quad (21)$$

The equations for variables $a(FC)$ and $b(FC)$ were then found using estimations and manual iteration-method to improve them, results are seen in figures 11-12. The modelled equations are eq.22-23.The irregular looking shape of the b-plot (figure 13) regarding the lab values was deemed to be caused by leakage behaviour in the drum caused by a shift from negative to positive gauge pressure. The model does not have to contain this anomaly as it is something that will not be expected to exist in the finished product.

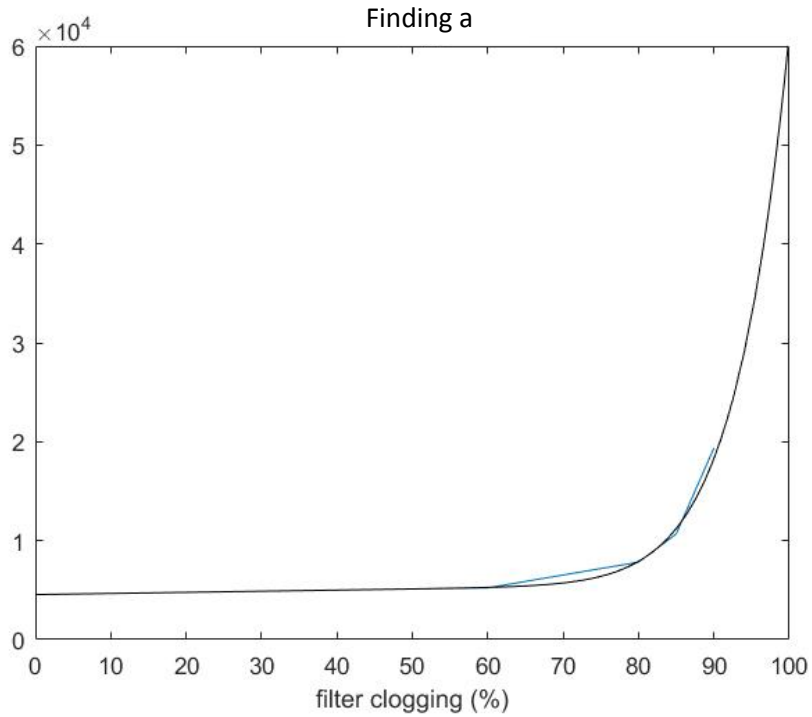

Figure 11 finding a, lab values (blue), model (black)

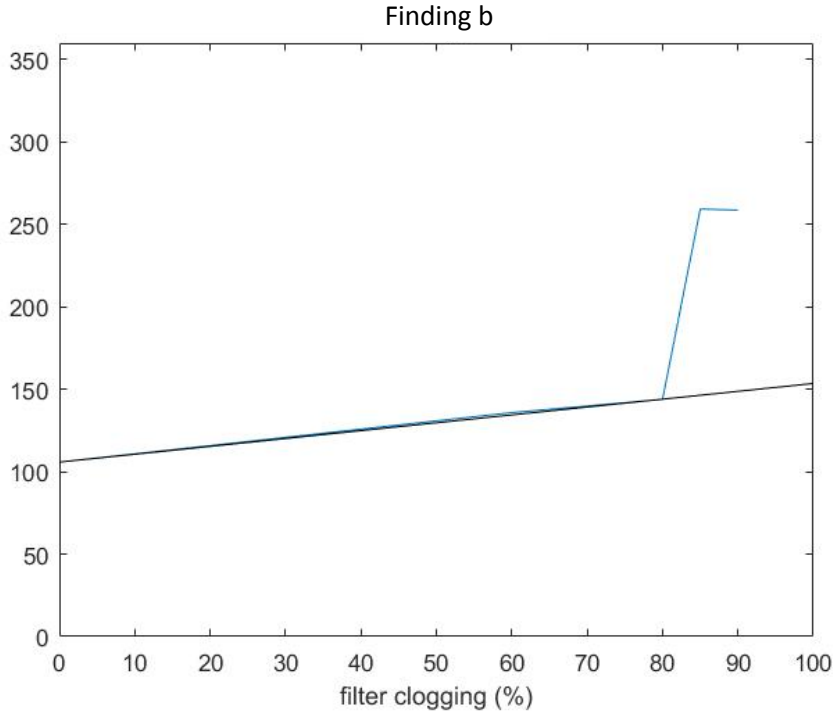

Figure 12 finding b, lab values (blue), model (black)

$$a = 4547 + 11.3544 \cdot (FC) + 110 \cdot (0.0156 \cdot (FC))^{14} \quad (22)$$

$$b = 105.8294 + 0.477 \cdot (FC) \quad (23)$$

The variable $a(FC)$ was modelled as an exponential function while $b(FC)$ was modelled as linear.

A stage has now been reached where Q, $P_{average}$ and P_{fan} can be modelled based on filter clogging and load as input variables. Following are two illustrations how Q varies with these input values.

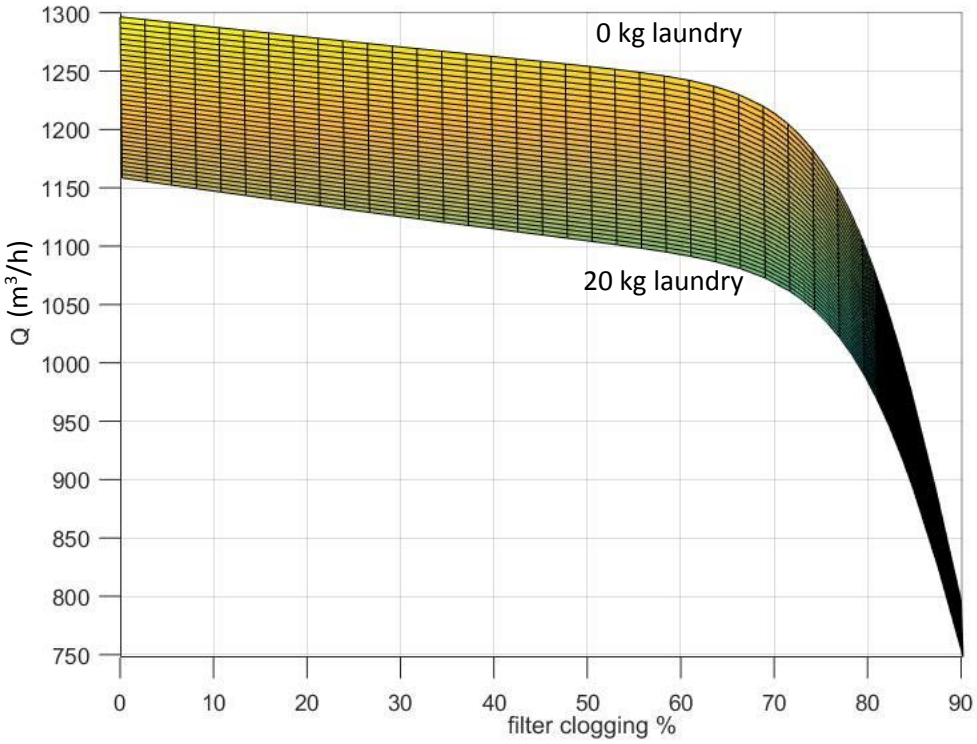

Figure 13 volume flow dependant on filter clogging %. Top and bottom of curve are extreme loads (0 and 20). 100kPa and 0˚C.

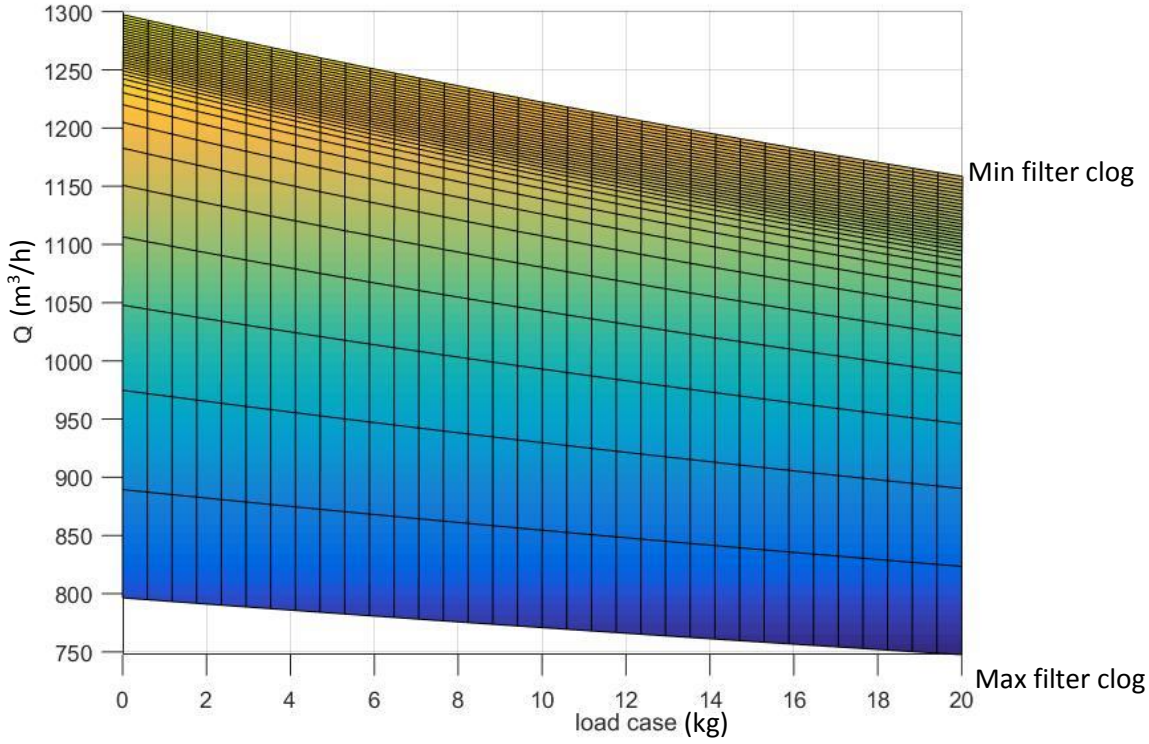

Figure 14 volume flow dependant on load in drum. Top and bottom are extreme filter clogging (0 and 90%). 100kPa and 0˚C.

A lot of the work is complete for the theoretical system model. Before moving on to studying individual components interaction, the overview of the first results can be analysed. It can be observed from figure 14 and 15 that going from 0 to 20kg laundry with a clean filter lowers the air flow Q from about 1300 to 1150 m^3/h normalized at 100kPa and 0˚C. Lower velocities can lead to less efficient laundry cycle. This kind of data could be used to get an overview of what the maximum acceptable load could be, assuming the trend continues in a linear fashion. However, before one makes any such assumptions it's important to note that the model is not calibrated for values outside the range.

As it regards the effects of filter clogging it can be seen that the flow changes substantially as the filter clogs up. Around 70% appears to be a tipping point where the volume flow starts to decrease rapidly. One weakness in this conclusion is that the method to represent a clogged filter was covering the filter with a flat plate, leaving 10% area open in one end. A more realistic experiment would have been some kind of porous plate with 10% holes spread evenly across the area. It's unknown if this approximation had a large effect on the lab result when comparing to a real filter clogged up with lint. For future studies one could study the effects of different ways the lint is distributed over the filter, either with the suggested porous plate or by moving the 10% opening to different places on the filter.

3.1.5 Component study.

To solve the remaining equations 8, 9, 10, 11 which are required to describe the load distribution across the components, the load distribution will be plotted based on the lab results. The following plots in figure 16 and 17 will be the pressure loss parameter k for each component divided by k_{load}. With equation 5 in mind, describing the total pressure loss as a sum of all the components pressure losses, this means $k_{component}/k_{load}$ was a normalized value of 0-1 describing how much part of the total system pressure loss is in that particular component. Again this is possible only because constant volume flow is assumed (no leakage). Solving a function for these normalized pressure loss parameters will mean the components pressure loss can easily be modelled as a product with P_{load} (currently already has a complete model).

The method for solving the normalized component pressure loss parameters is similar to studies of $P_{average}$ and k_{load} in subchapter 3.1.2 and 3.1.3 However on this component study linear equations can no longer be assumed. The method is still to find an initial value based on filter case and then a varying part based on filter and load case. Figure 16 shows the initial pressure loss for each component with fixed load=0 and filter clogging 0-90%.

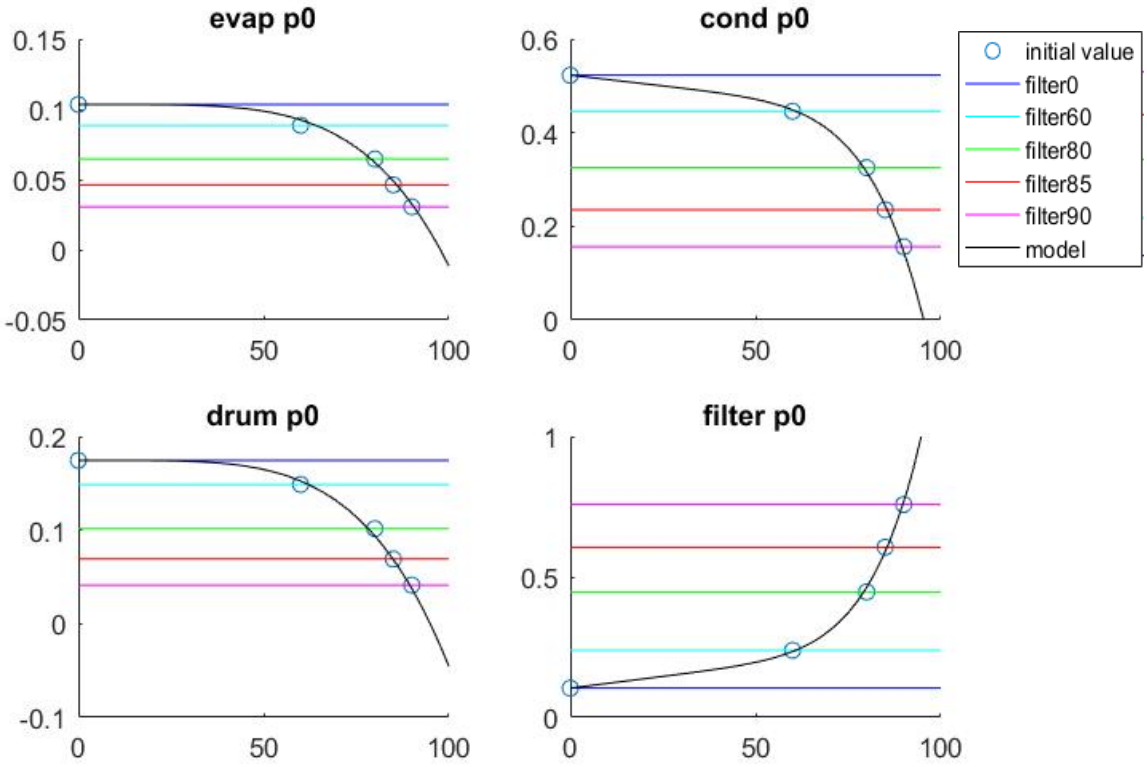

Figure 15 initial values for normalized pressure loss parameters on y-axis and on filter clogging (%) x-axis. The "model" plots in black are curves fitted to the experimental results (initial value), and the modelled functions for these are in equations 24-27. The horizontal lines for the filter cases are purely illustrative to make the corresponding values on y-axis more readable.

$$K_{start\_evap} = 0.102 - \left(\frac{(\mathrm{FC})}{160}\right)^{4.6} \tag{24}$$

$$K_{start\_cond} = 0.5227 - \left(\frac{(\mathrm{FC})}{108}\right)^{6.7} - (\mathrm{FC})/1100 \tag{25}$$

$$K_{start\_drum} = 0.1745 - \left(\frac{(\mathrm{FC})}{140}\right)^{4.5} \tag{26}$$

$$K_{start\_filter} = 0.1043 - \left(\frac{(\mathrm{FC})}{99}\right)^{7} + (\mathrm{FC})/600 \tag{27}$$

Functions 24-27 were found using manual iterative improvements. They are all of similar nature, containing a constant, and exponential part and a linear part. One of the goals that Electrolux had for this thesis was to investigate the possibility of making the theoretical modelling of tumbler systems into some kind of automated system using lab data as an input. So far the functions have been mostly of similar structure and it would not be impossible to find these models using some kind of program, such as Matlab with an iterative polyfit script, trying different degrees of exponential functions until acceptable accuracy has been achieved. For the next part of the component study, the variable load is introduced. Completing the functions for the modelled normalized pressure loss parameter for the different components is still the goal, but now varying load is introduced.

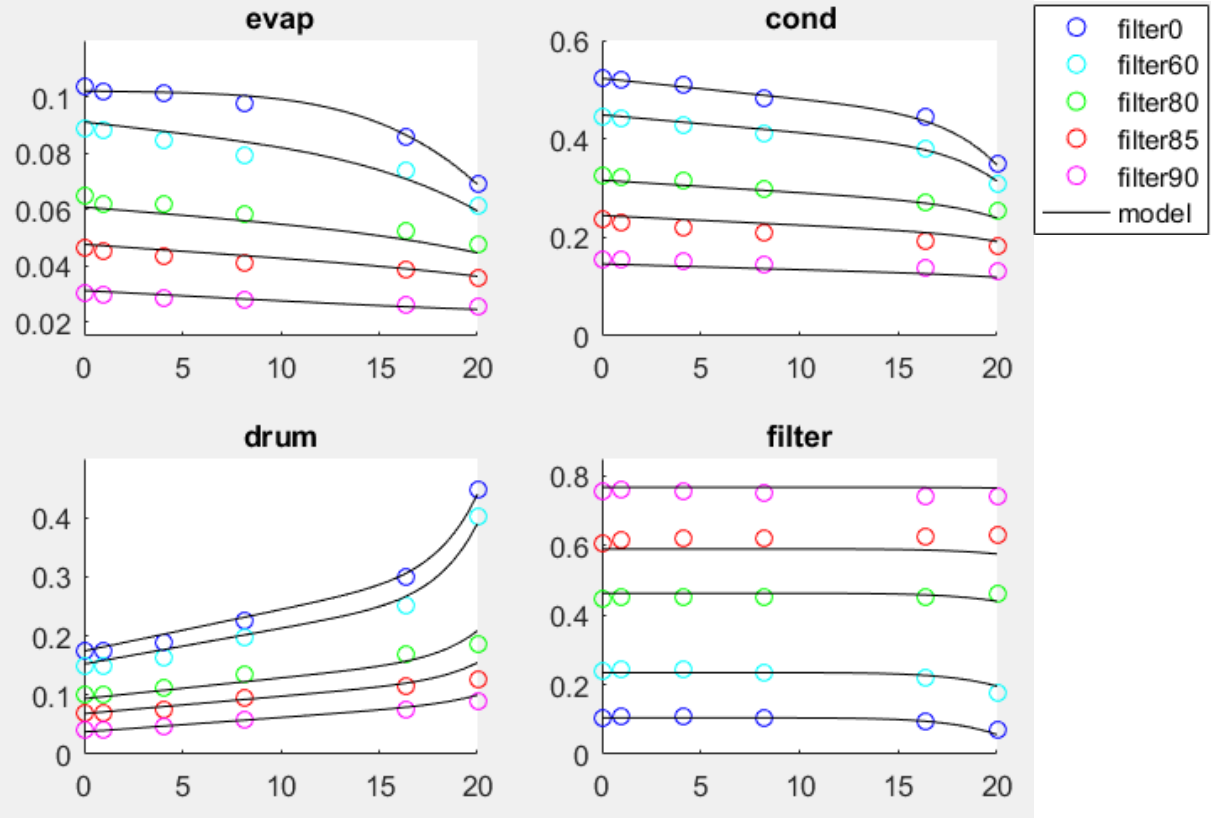

Figure 16 load (kg laundry) on x-axis, normalized pressure loss parameter on y-axis

This was the hardest part yet to find models to fit all lab values for the different filter clogging cases simultaneously. The model functions adapted from figure 17 can be seen in eq.28-31.

$$K_{evap} = -\left(1 - \frac{(FC)}{50}\right)^2 \left(0.015\frac{LF}{20}\right) - 0.01\left(\frac{LF}{20}\right)^4 - 0.002\left(\frac{LF}{20}\right) - 3K_{start\_evap}{}^6 + K_{start\_evap} \quad (28)$$

$$K_{cond} = -0.1\left(\frac{K_{start\_cond}}{0.54}\right)^{2.5}\left(\frac{LF}{20}\right)^8 - 0.16 \cdot K_{start\_cond}\left(\frac{LF}{20}\right) + \cdot K_{start\_cond} \quad (29)$$

$$K_{drum} = \left(1 - \left(\left(\frac{FC}{50}\right)^2 - 1\right)^2 0.08\left(\frac{LF}{20}\right)^{10} + 0.05\frac{LF}{20} + 0.5cos^2\left(FC\frac{\pi}{200}\right)\right)\left(0.25\left(\frac{LF}{20}\right)^{10} + \frac{LF}{100}\right) + \frac{LF}{500} + K_{start\_drum} \quad (30)$$

$$K_{filter} = \left(-0.055 + 0.06875(FC)\right)\left(\frac{LF}{20}\right)^8 + K_{start\_filter} \quad (31)$$

This part of the theoretical modelling required a lot of iterations until a suitable solution was achieved. Unconventional method compared to the earlier modelling was used in that the start

values for the load free case were used as an input for eq. 28 and eq. 29. Looking at the final result it's easy to conclude that they could have been simpler in their format, and contains a lot of complicated parts. A generic script or code could never come up with results like these. There might be easier solutions that are more accurate. These functions will suffice for the Theoretical model prototype though. Now all the components are in place to write a script describing the whole system with load distribution and gauge pressure in all components.

3.1.6 Application of theoretical system model

With the Matlab model prototype complete it is time to investigate its implications and uses. As suction to the surrounding is desired in the drum to prevent leakage at the hatch, the 0 point in gauge pressure is of interest. The model can be adjusted to cover any input values for filter clogging and laundry load in drum. However the accuracy will probably decrease drastically if values outside the calibrating range are used. For example if it's used for 40kg of laundry, unpredicted effects may occur as no such extreme experimental data was used.

In the following figures, some 3d plots will be made using the model to illustrate one way to use the model. The plots have been turned and cut with a plane at P=0 to show where the suction/over pressure transition is located.

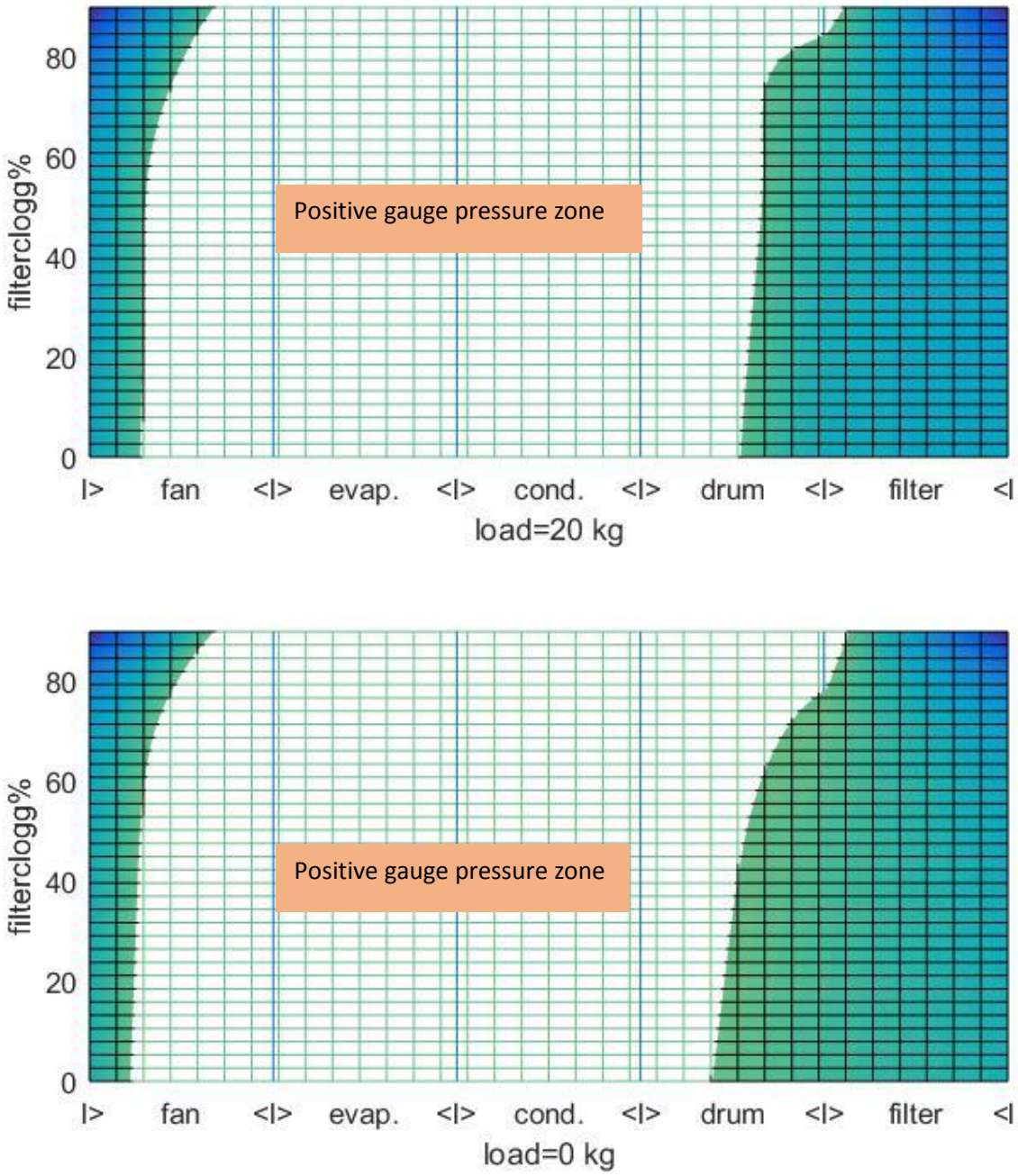

Figure 17 Position of zero point of gauge pressure for varying FC but for two constant extreme loads: 20kg load (top) and 0kg load (bottom)

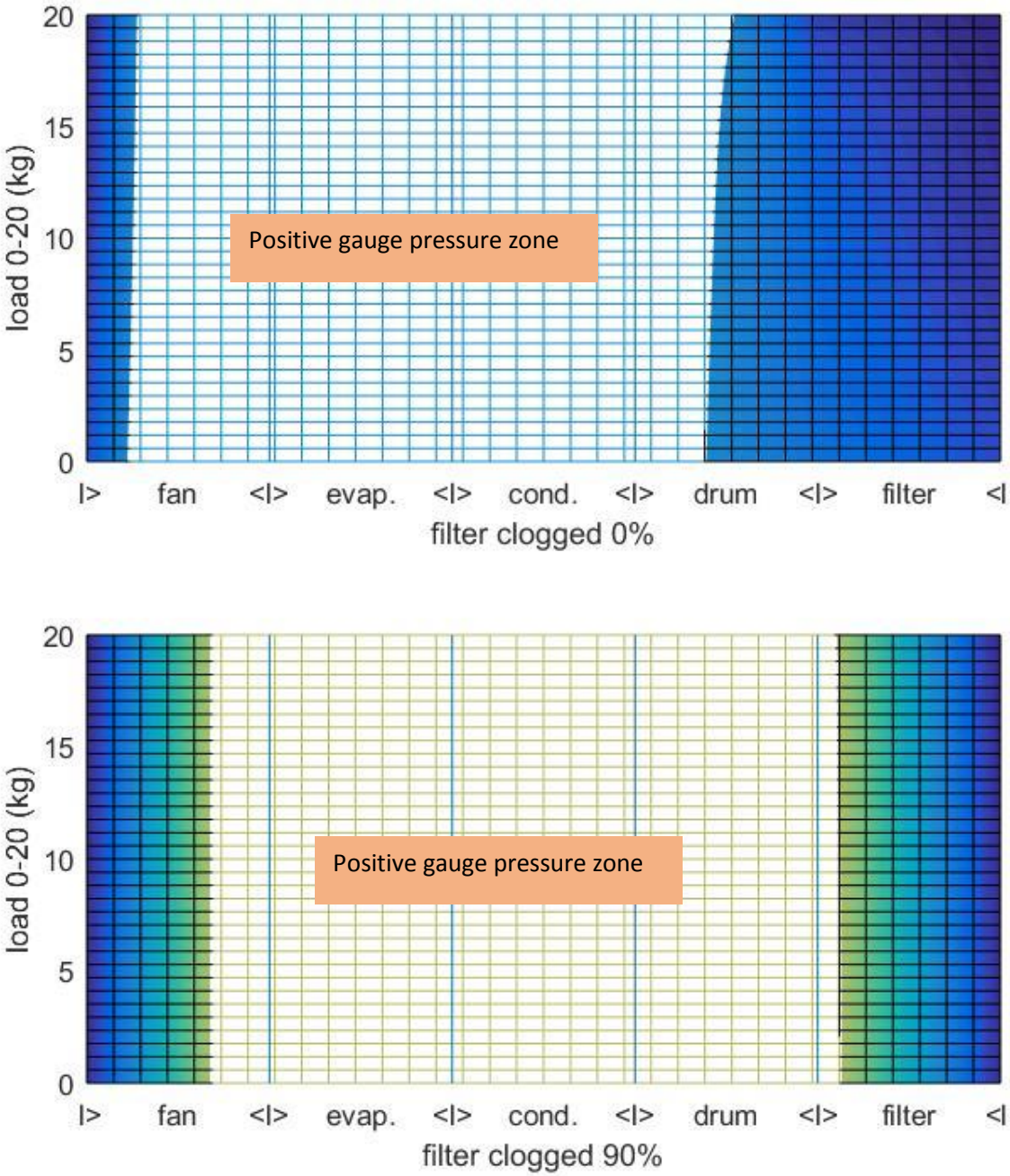

Figure 18 Position of zero point of gauge pressure for varying loads with two constant extreme FC cases: 0 clog (top) and 90% clog (top).

In figure 17 two plots can be observed. These have filter clogging varying between 0-90%. From the top-most plot with 20kg load, it can be observed that the zero gauge pressure point is moved forward into the filter for 80% and higher filterclogg. This leads to a high leakage and bad performance as no suction occurs in the drum.

For the 0kg load, the 0 gauge pressure point reaching into the drum actually occurs earlier at roughly 70% filter clog. However at 0 load and 0 filter clog the gauge pressure zone is further back in the drum than 20 kg load 0% filter clog. Such an effect is easy to spot in this illustration but might be harder to detect just looking at the lab data. The theoretical model gives an indication of how the system should behave in the relatively long intervals between measurement points. There is no guarantee that there are no unpredicted variances for those intervals, however, it is highly unlikely.

In figure 18 the filter clog is left constant while the load varies. This can be observed to have little relevant effect on the location of the positive gauge pressure zone. This is especially true for the case with the 90% clogged filter.

Figure illustrates the same effects as figure 17-18, but for individual cases instead.

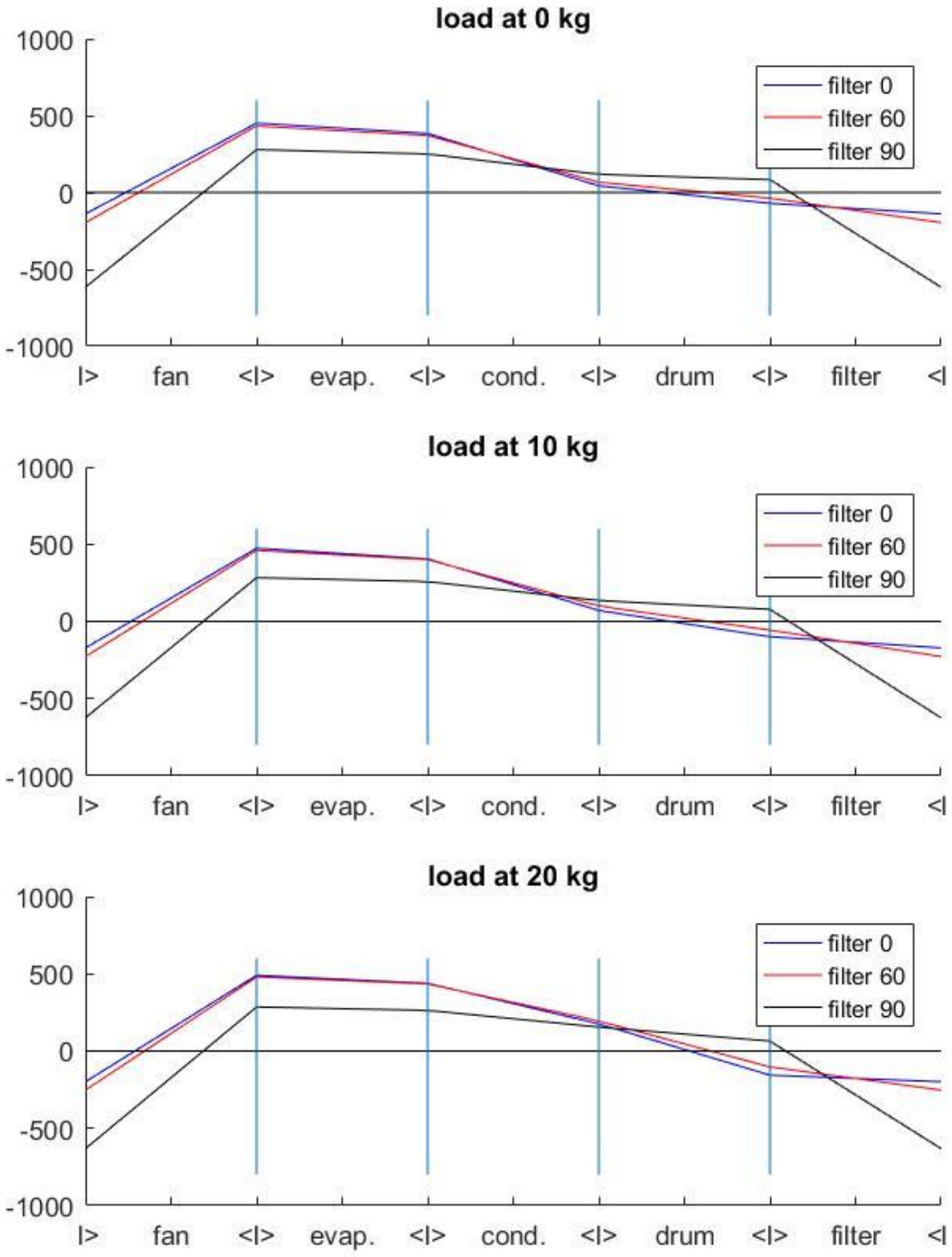

Figure 19 Gauge pressure along the system for some different load cases: filter clogged to 0 (blue), 60 (red) and 90% (black) for 0kg (top), 10kg (middle) and 20kg (bottom).

In figure 19 it can be observed that for all load cases the filter clogging changes little at 0-60 range. Changes becomes a lot more apparent when closing upon the extreme cases, and the one at 90% clog can clearly be seen to be different from the 0-60% clog. What can also be observed is that increased levels of filter clogging pulls down the average pressure (pressure in the middle of the fan). However this does not help in achieving vacuum gauge pressure for the drum since most of the pressure drop occurs near the filter in those cases.

3.2 CFD simulation model and complementing lab measurements.

With the theoretical model complete, it's time to move on to the CFD-simulation of the heat pump part of the airflow geometry. The first task was to collect new lab data to help with selecting the input values for the CFD.

3.2.1 Data from lab measurements made to help in building the simulation model

Table 3 Measured overall pressure and flow using the lab rig. Standard deviation is based on 30 averages of 10 values each.

	Measured airflow		Average static pressure			Standard deviation		
Low load	Nm3/h	(m/s) @ inlet	A	C	E	A	C	E
No compressor	1107.61	1.97	363.06	327.39	40.04	4.54	4.48	1.73
With compressor	1113.18	1.98	365.22	325.51	39.74	7.40	7.81	1.96
High load								
No compressor	680.27	1.21	172.31	153.37	15.72	6.18	5.64	3.28
With compressor	681.88	1.21	171.11	150.96	15.72	5.00	4.68	3.28

The goal with the flow cases was to represent the low load no filter case and the high load clogged filter case. The normalized air conditions (100kPa, 0˚C) meant that the volume flows aimed for was roughly 1150-and 640m^3/h. The airflow was difficult to regulate, using a flat plate to partially cover the filter and inlet to fan. The results in table 3, is as close to the relevant cases as it was achievable at the time. The values at plane A, C and E will be used to calibrate the porous media representing the heat exchangers to be of appropriate density/resistance.

In table 4, data for local velocities was collected from the lab rig along the metal rod traverses. The traverses was placed to make sure the pitot static tubes were fixed in the flow direction. The measured direction was upwards (z-axis) in plane C and forwards (x-axis) in the plane E. The points along the traverses are equal distance apart and start near the shell of the geometry. The velocity measurements were meant as a final comparison with the simulation results and reality. It can be observed that the standard deviation was high for these lab measurements, but it was hard to get stable results when measuring the low velocities using the Pitot static tubes. The instruments took 300 measurements per test for table 4. However the instruments reported data as 30 output values consisting of averages for 10 values each. This leaves the average values of velocity correct but it might skew the variance, which makes the standard deviation (presented here to indicate accuracy of measurements) possibly underestimated. As the variance within the averaged values are unknown though, this cannot be proved.

The high standard deviations for the lab measured made with pitot static tubes for the velocity profiles hints that this method to validate the CFD is not good. But to check that statement further, the comparison will proceed.

Table 4 Measured airflow from the lab rig. Standard deviation is based on 30 averages of 10 values each, the amount of samples for each value was 300. The points are tagged with names 0-4 or 0-2 and are placed equal distance apart along axis x, y or z in the direction as seen in the leftmost cell.

		No compressor 2m/s		No compressor 1.2m/s		Compressor 2m/s		Compressor 1.2m/s	
placement		Velocity (m/s)	Standard deviation (m/s)	Velocity (m/s)	Standard deviation (m/s)	Velocity (m/s)	Standard deviation (m/s)	Velocity (m/s)	Standard deviation (m/s)
C Side y -> -y	0	1.41	1.79	2.54	1.67	1.13	1.72	2.00	1.57
	1	-0.53	2.21	1.94	1.75	-0.24	1.91	2.25	1.35
	2	-1.98	1.68	2.02	1.76	-1.65	1.59	1.50	1.88
	3	-0.18	2.11	2.29	1.69	0.98	1.78	2.58	1.47
	4	0.05	2.23	2.51	1.69	0.91	2.10	1.88	1.79
C Front -x->x	0	3.27	1.19	3.33	0.99	3.13	1.01	3.49	0.81
	1	-0.50	2.35	1.91	1.93	-1.42	1.70	2.31	1.34
	2	-1.77	1.55	2.05	1.73	0.04	2.01	1.89	1.74
E Side y -> -y	0	7.42	0.33						
	1	6.04	0.42						
	2	7.02	0.38						
	3	7.42	0.37						
	4	8.01	0.30						
E Top z >-z	0	7.75	2.28						
	1	7.37	2.06						
	2	7.53	2.36						
	3	7.57	2.72						
	4	2.82	2.10						

3.2.2 Grid sensitivity study

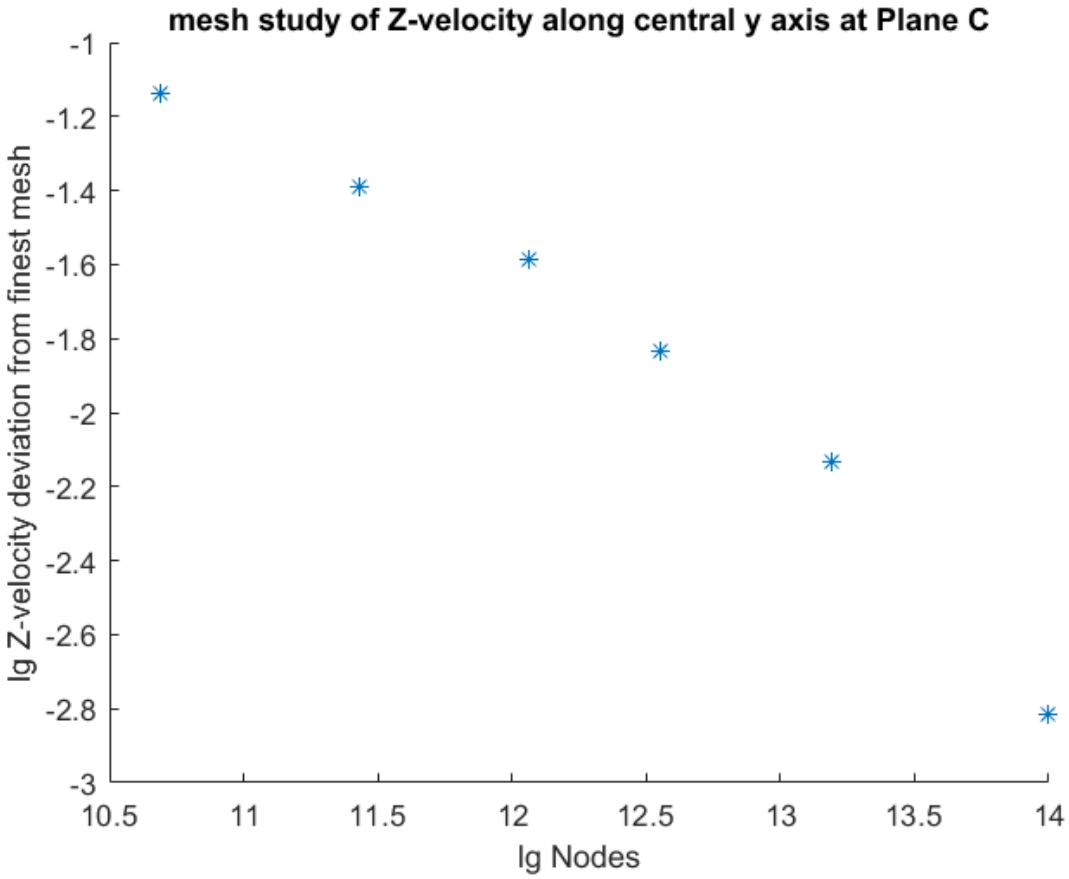

Figure 20 mesh study- this shows how increasing amounts of nodes converges results closer to the finest mesh.

Figure 20 illustrates how the accuracy of the simulations approach the results of the finest mesh. The Z-velocity profile along the y-axis at Plane C was used. This is at the inlet to the condenser (see figure 4 for further clarification). 10 points along that line was used to quantify the deviation as follows in equation 32. In eq.32 *i* is the point along the y-axis, *m* is the choice of mesh and *m_f* is the finest mesh. *V* is the Z-velocity and *N* is the amount of points.

$$deviation = \sqrt{\sum_{1}^{i=10} \frac{\left(V_{im} - V_{im\_f}\right)^2}{N_i}} \quad (32)$$

It can be observed in figure 20 that the trend is converging, indicating the difference between different grid results gets closer to the solution of the finest grid as the amount of nodes increases. The time needed for calculations also increases though, especially when generating the grids. Mesh 6 was selected (the rightmost value in figure 20) to keep the time needed to build and simulate all grids reasonable. The grid study indicates that a deviation of roughly 2.5% for the Z-velocity profile compared to the finest mesh remains.

To further investigate mesh independence, a quick experiment further refining the mesh using mesh adaptation to reduce y+ was tested for mesh 4. This made 0.04% difference which is deemed to be of no concern. A different turbulence model was tested for the final mesh 6. The k-omega SST model gave a 0.6% difference in inlet area weighted pressure. With effects of grid size, mesh adaptation and an alternative turbulence model tested, mesh 6 with the k-epsilon turbulence model and no further mesh adaptation was deemed a sufficiently independent solution.

3.2.3 CFD simulation result validation and compressor effects on pressure losses.

In the following table are the calibration results for the high velocity case, and the simulation results for the low velocity case. These results will indicate how the model including porous region holds up under changing conditions. The top tables are the CFD and the bottom ones are from the lab measurements. Also the case with no compressor and with compressor are both included as suggested for the geometry improvement part.

Table 5 Comparison of lab measurements and CFD results (CFD-model build from LOW LOAD case with high accuracy). CFD-model overestimates pressure by roughly 24% for high load cases compared to lab

Simulation result at 0 ref. pressure outlet	Inlet airflow (m/s)		static pressure (Pa)		
LOW LOAD			inlet	between HEX	outlet
no compressor	2		324	287	0
with compressor	2		333	285	0
HIGH LOAD					
no compressor	1,2		189	168	0
with compressor	1,2		192	167	0

Lab result at 0 ref. pressure outlet	Inlet airflow (m/s)		static pressure (Pa)		
LOW LOAD			inlet	between HEX	outlet
no compressor	1,97		323	287	0
with compressor	1,98		325	285	0
HIGH LOAD					
no compressor	1,21		156	137	0
with compressor	1,21		155	134	0

The airflow is assumed constant for both CFD and lab results. As mentioned in the method part, centrally placed Pitot static tubes were used to measure static pressure as close as possible to the inlet of HEX1, inlet of HEX2, and at the outlet of heat pump geometry (Plane A, C and E in figure 4).

When calibrating the resistance in the porous zone for the heat exchanger parts, lab results for low load case (@ roughly 2m/s) were used. It can be observed that high accuracy (0-2% deviation) was achieved for the calibration. However, when translating the model to a high load case (roughly 1.2 m/s) the pressure loss becomes higher for the simulation than the lab results. The difference of 21-23% is too high to explain by results inaccuracies in the lab. In fact, since velocity was rounded down for the simulation, the pressure should be lower than compared to lab results. The reason for the difference is likely that the porous zone model is not a perfect approximation of the real heat exchangers. In the future it is recommended to calibrate the porosity to at least two different measured cases and replace the constant porosity used herein by a variable one. This could be achieved by having the resistance of the porous medium as a user defined function.

Of note in table 5 is also the effects of the compressor. In the experimental measurements the compressor appeared to have no noticeable effect on the overall pressure loss (+-0.6% for the inlet pressure in both high and low load cases). In the simulation, the difference is still minor of +-2-3% inlet pressure, but slightly increased compared to the measurements. That can be explained by the geometry of the compressor approximation to have sharp edges, while the real one is a lot smoother, which could lead to increased turbulence created in that region for the CFD compared to the lab conditions.

3.2.4 Visual overview of the CFD simulation results of compressor effects on low load cases.

In figures 21-26, different visual plots of the flow behaviour are plotted. Figures 21-23 are for the geometry with the compressor and figures 24-26 are for the geometry without the compressor. Both are for the low load high velocity case (0kg, 0% filter clog, 2m/s inlet velocity). This case has been chosen as the high velocity should provide maximum amount of aerodynamic pressure losses for the heat pump part of the geometry. Three types of plots are provided to highlight different effects.

1. Velocity magnitude plots. These are useful to identify wake regions (blue) where the flow has formed recirculation zones. These regions are generally unwanted as energy is lost to introduce turbulence into the flow and cross section flow area is reduced, leading to locally high velocities and as a consequence increased friction losses.
2. Turbulence kinetic energy (k). This indicates where the flow has had its turbulence increased, which can happen at sharp edges for example in the geometry. These effects are undesired when pressure loss is sought to be minimized.
3. Pressure distribution inside the geometry. This is useful to get an overview of where the majority of the pressure loss is introduced to the flow.

The geometry after the outlet can be discarded as the extension is just to make the solution more stable. To make the remaining part of the geometry more clearly viewable but to also keep the general shape of the simulation geometry visible, the extreme values have been cut to range.

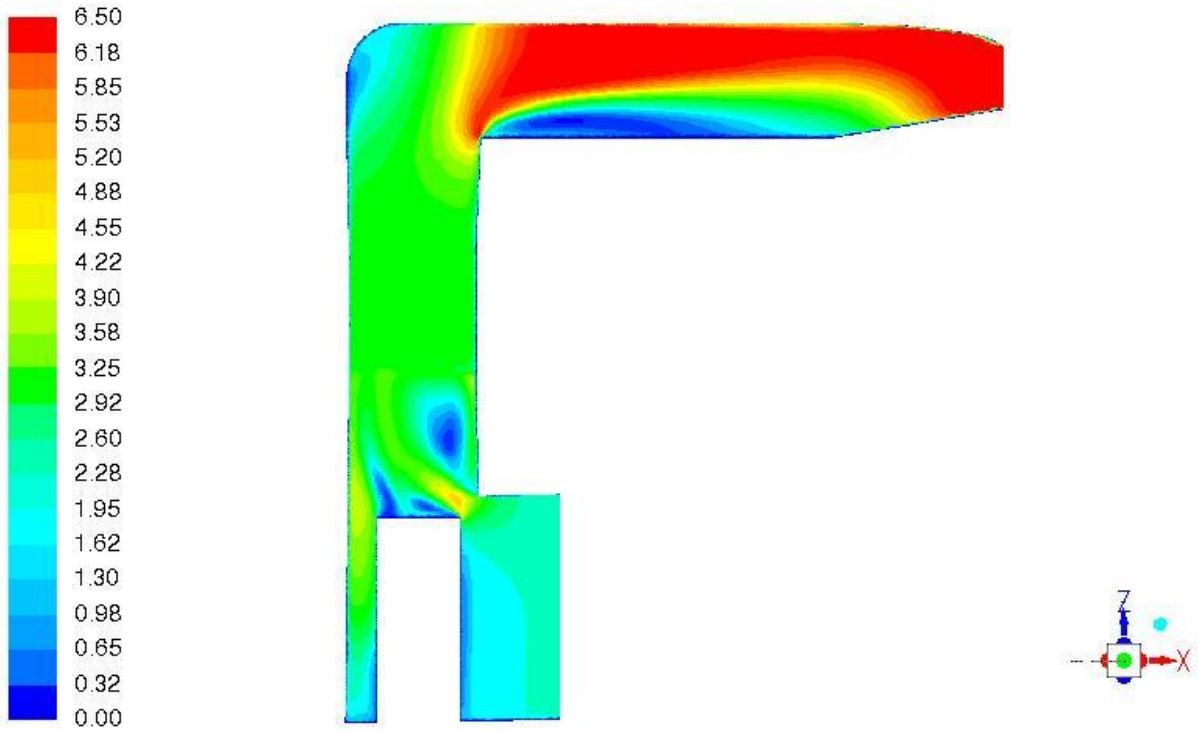

Figure 21. Velocity magnitude for 2m/s case. Values above 6.5 have been clipped to range

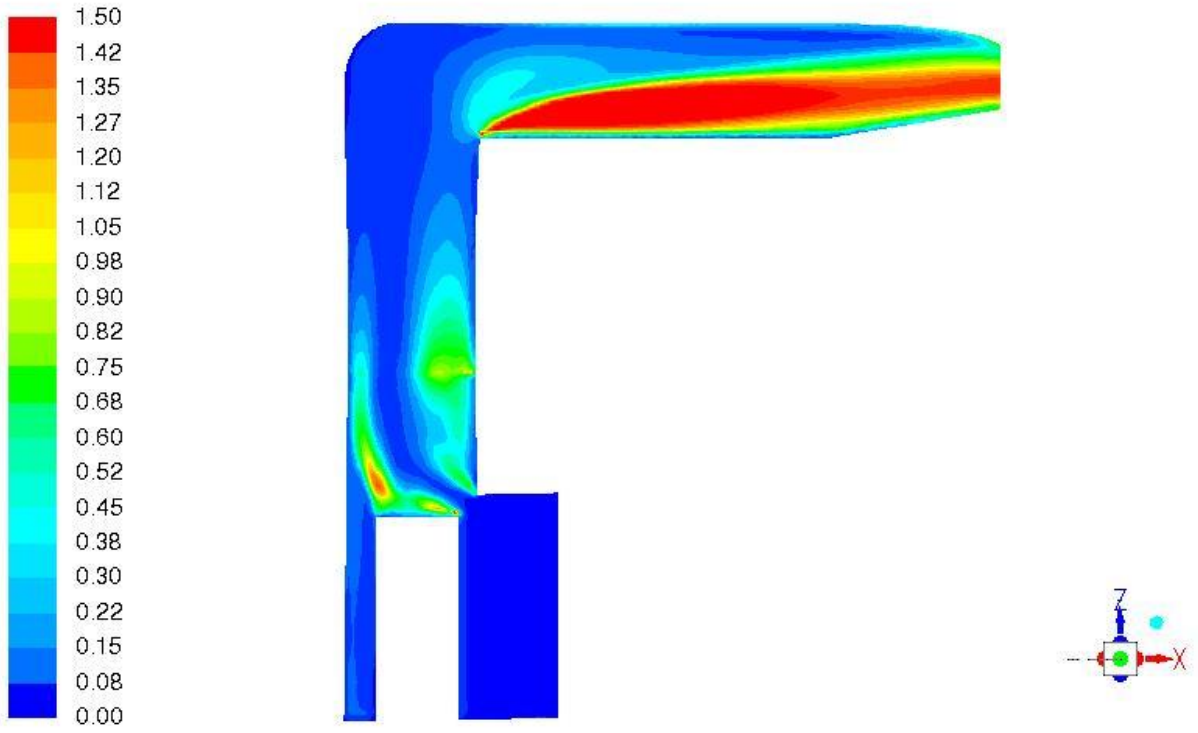

Figure 22 k magnitude for 2m/s case. Values above 1.5 have been clipped to range

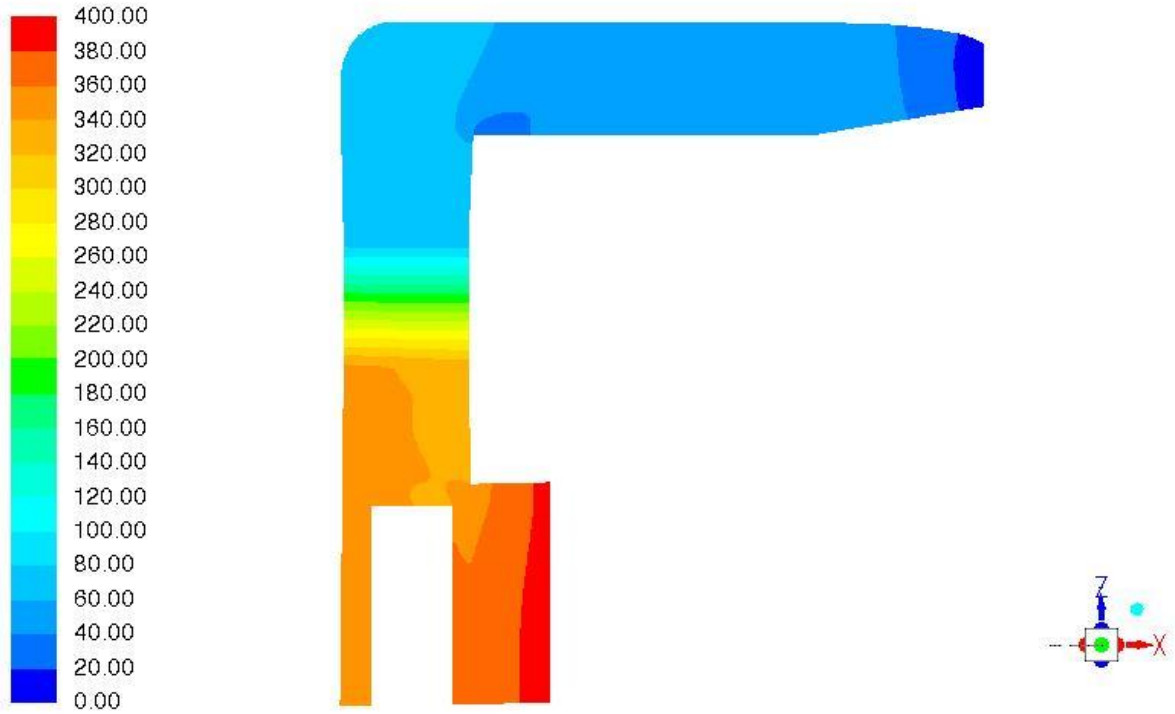

Figure 23 pressure magnitude for 2m/s case. Values above 400 have been clipped to range

From figure 21 it can be observed that there are recirculation zones (darker blue) at the bend after the inlet, at the bend before the outlet and at the top of the compressor. As stated recirculation zones are not desired when minimizing pressure losses. To prevent recirculation zones from forming at these edges, the geometry could be smoothed out at those edges. Figure 22 shows the turbulence kinetic energy (k). It can be observed that k is higher at the former mentioned recirculation zones. This energy directly contributes to higher flow resistance, as the energy required to maintain the vortices are absorbed from the kinetic energy of the airflow.

Figure 23 shows how the pressure changes throughout the system. From this it is hinted that most of the pressure loss comes from the heat exchangers, and not the actual geometry. To maintain a good heat exchange, wall contact is required. This part can therefore not easily be optimized to reduce pressure loss. Since so little pressure is changed outside of the heat exchangers, the question is raised of the relevance to optimize flow geometry and how those gains would compare to the overall system losses. The relevance is investigated more detailed further on in table 9.

In figures 24-26 the same conditions apply as in figures 21-23, but these are for the geometry with compressor removed.

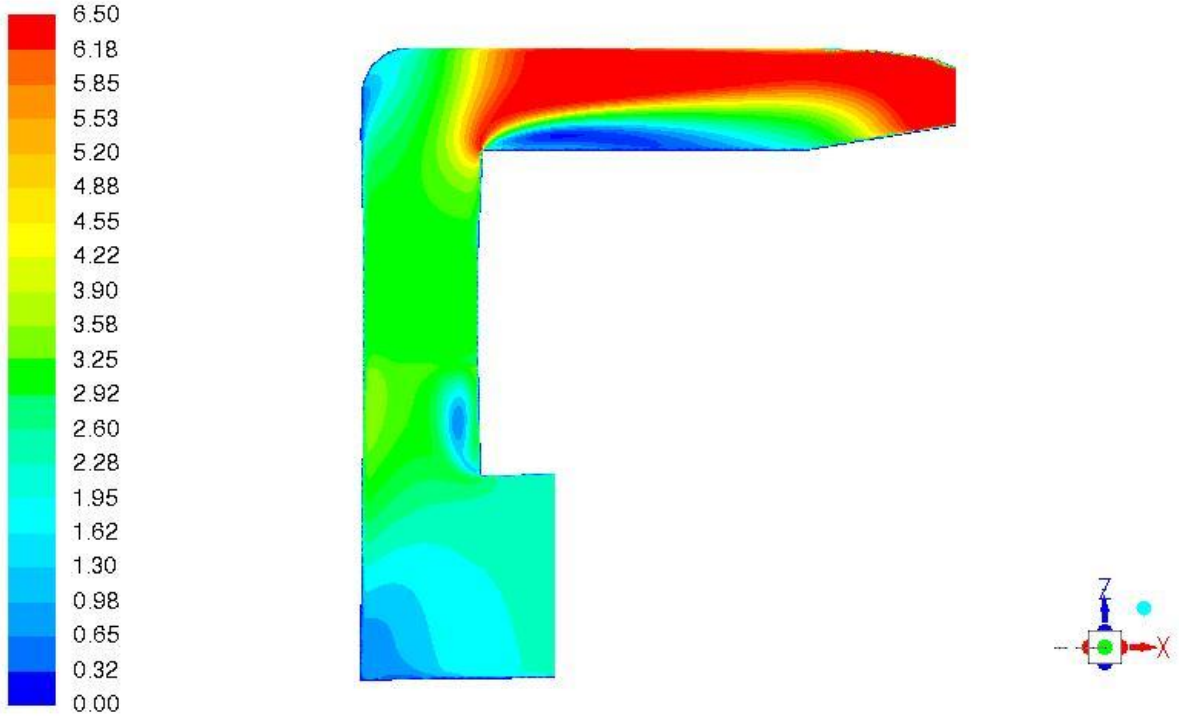

Figure 24 Velocity magnitude for 2m/s case. Values above 6.5 have been clipped to range

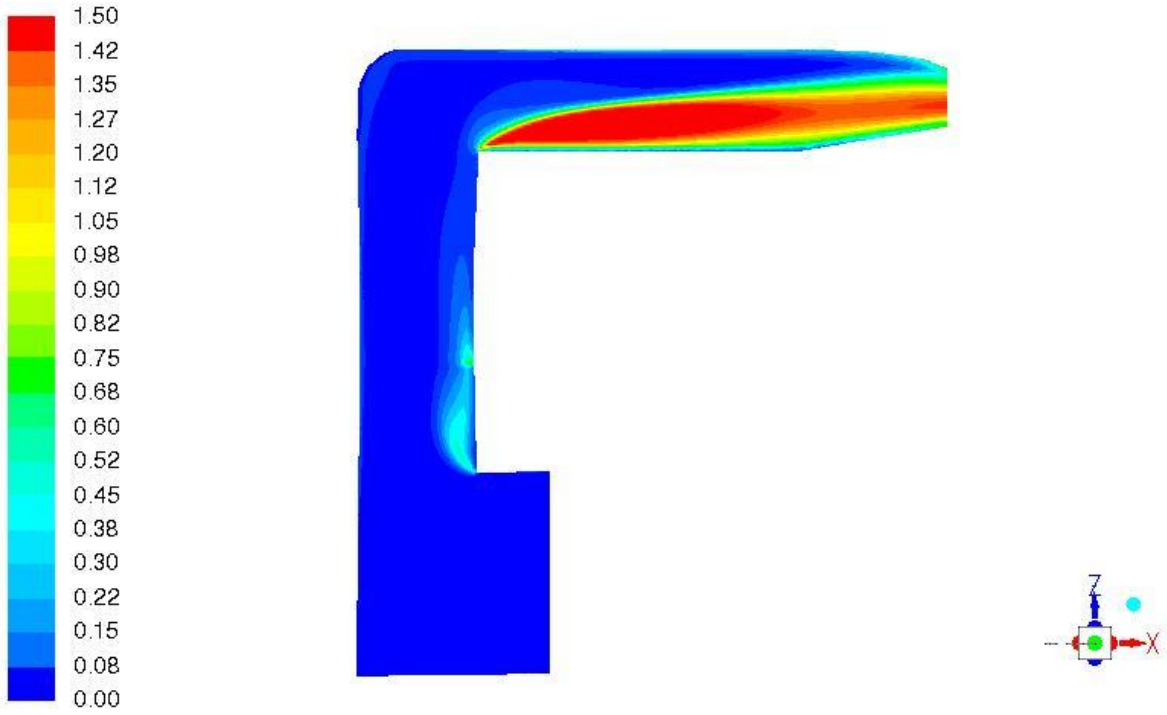

Figure 25 k magnitude for 2m/s case. Values above 1.5 have been clipped to range

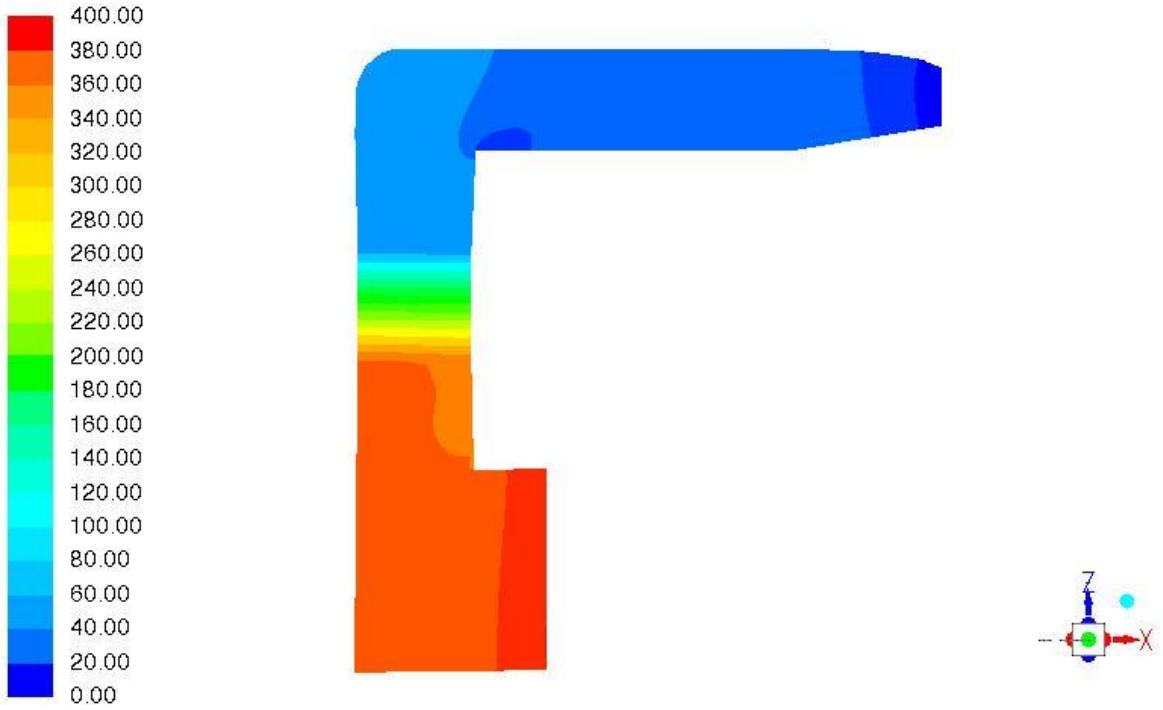

Figure 26 Pressure magnitude for 2m/s case. Values above 400 have been clipped to range

Figure 24 indicates that there are less recirculation zones close to the inlet. Figure 25 shows that there is also less turbulence throughout the geometry, but in particular close to the inlet as near the inlet without the compressor.

However, looking at figure 26 it appears that removing compressor and getting reduced turbulence had had no major visible effect on the overall pressure loss. This is in line with the results already seen and discussed in table 5. These results together confirm that the compressor had no relevant effect regarding the pressure loss. Logically it can be assumed that the compressor would have an even smaller effect for the high load case as the air velocity would be slower, making all wake regions and friction effects smaller.

3.2.5 Initial result for validating velocity profiles with lab measurements.

The lab measurements along traverses were made to validate the CFD simulation results. In figure 27 velocity profile are plotted at plane C (inlet to HEX 2, see figure 4). The CFD velocity profile at C is plotted in red. The lab measurements and their standard deviation is plotted in green. The Pitot static tube had a length of roughly 5mm which was limiting when trying to measure velocity at the HEX 2 inlet (such a velocity profile is of interest for the goal to study velocity distribution at the HEX). Therefore CFD results are also plotted (blue) for a profile 5mm below plane C to be more closely comparable to lab measurements.

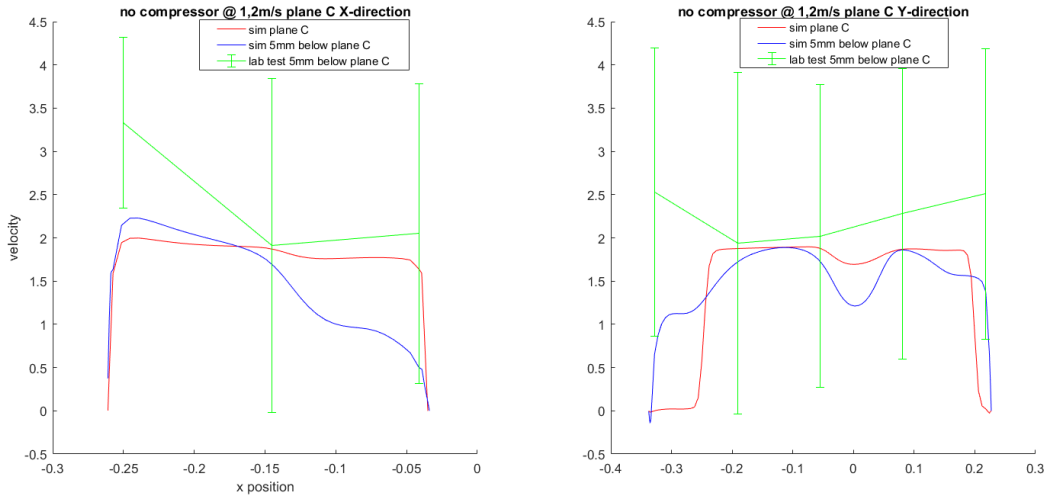

Figure 27 velocity profile and lab results along two lines in plane C (inlet to HEX2). The lab result plot has error bars indicating standard deviation. It can be observed that these standard deviations are exceptionally large.

For clarity's sake the error bars showing standard deviation will not be plotted in the next subchapter. Figure 27 indicates that the lab measurements should not be trusted to give a believable velocity profile as the variance in the results were exceedingly high compared to the velocity of the flow. This was true for all cases as could be predicted previously when studying table 4. To counter this issue the lab measurements could have consisted of more data values, or other more precise measurement instruments should have been used.

3.2.6 Flow uniformity and CFD velocity profile compared to Lab measurements.

In the following study, the simulation results of all 4 cases (low load, high load, compressor and no compressor) at plane C for the z-velocity will be compared. Only 2 cases are plotted as they are all fairly similar (figure 29 and 31) the rest of the plots can be found in appendix A and B. Also the lab results will be compared to these simulation results in the same fashion as the subchapter 3.2.5. These profile along X and Y direction will be complemented by a full view of the axial flow for plane C for clarity (figure 28 and 30).

Plane C 2 m/s no compressor case plots

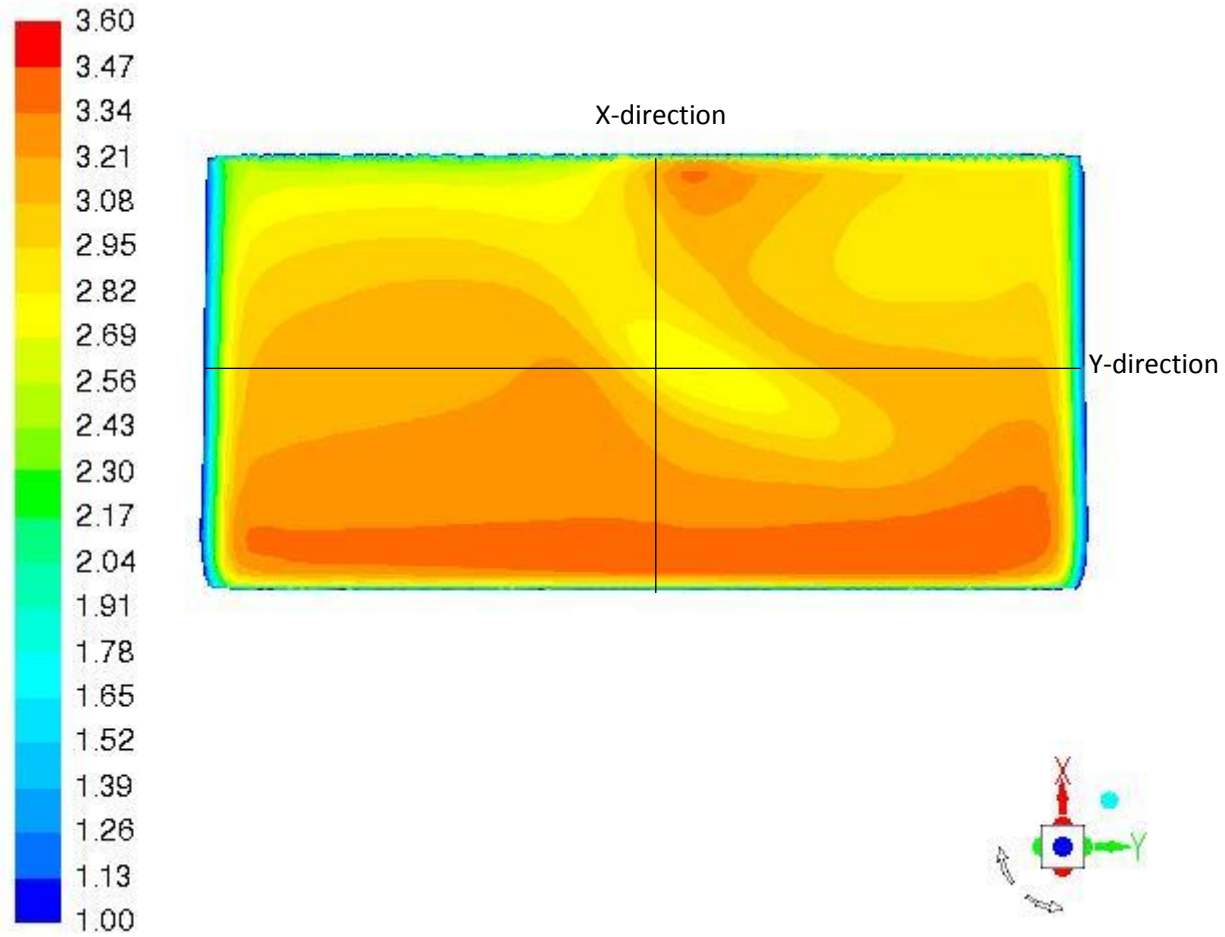

Figure 28 Full view of Z-velocity for the airflow at plane C. The black lines indicate where the velocity profiles are plotted.

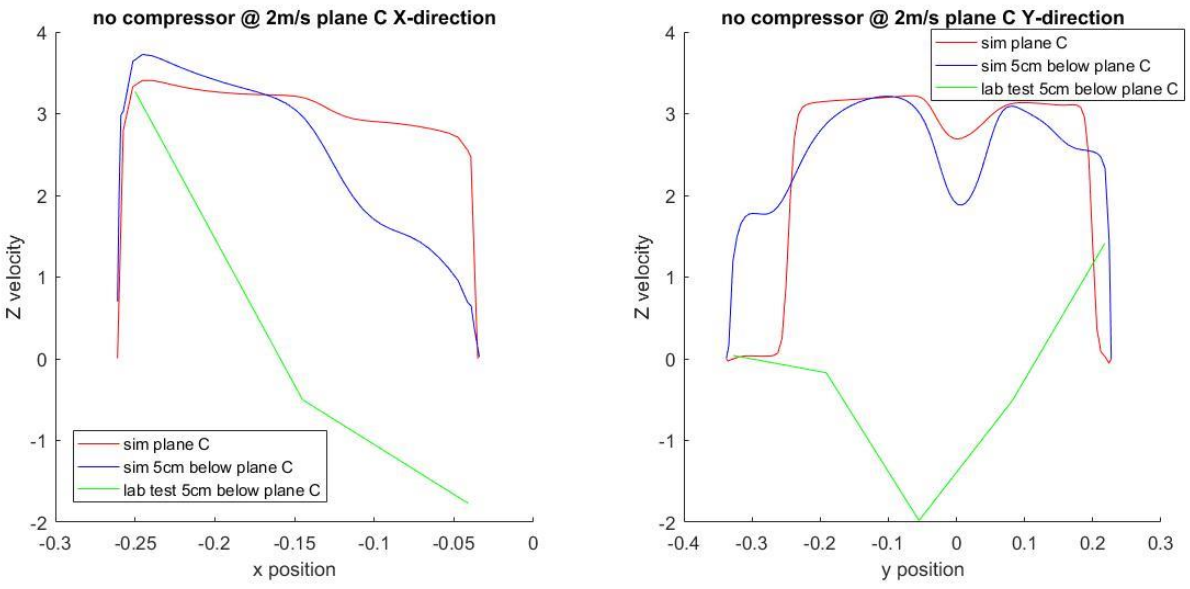

Figure 29 Z-velocity profiles along central axis in x- and y-direction. The red and blue lines are CFD results. Green line is lab measurements

Plane C 1.2 m/s with compressor case plots

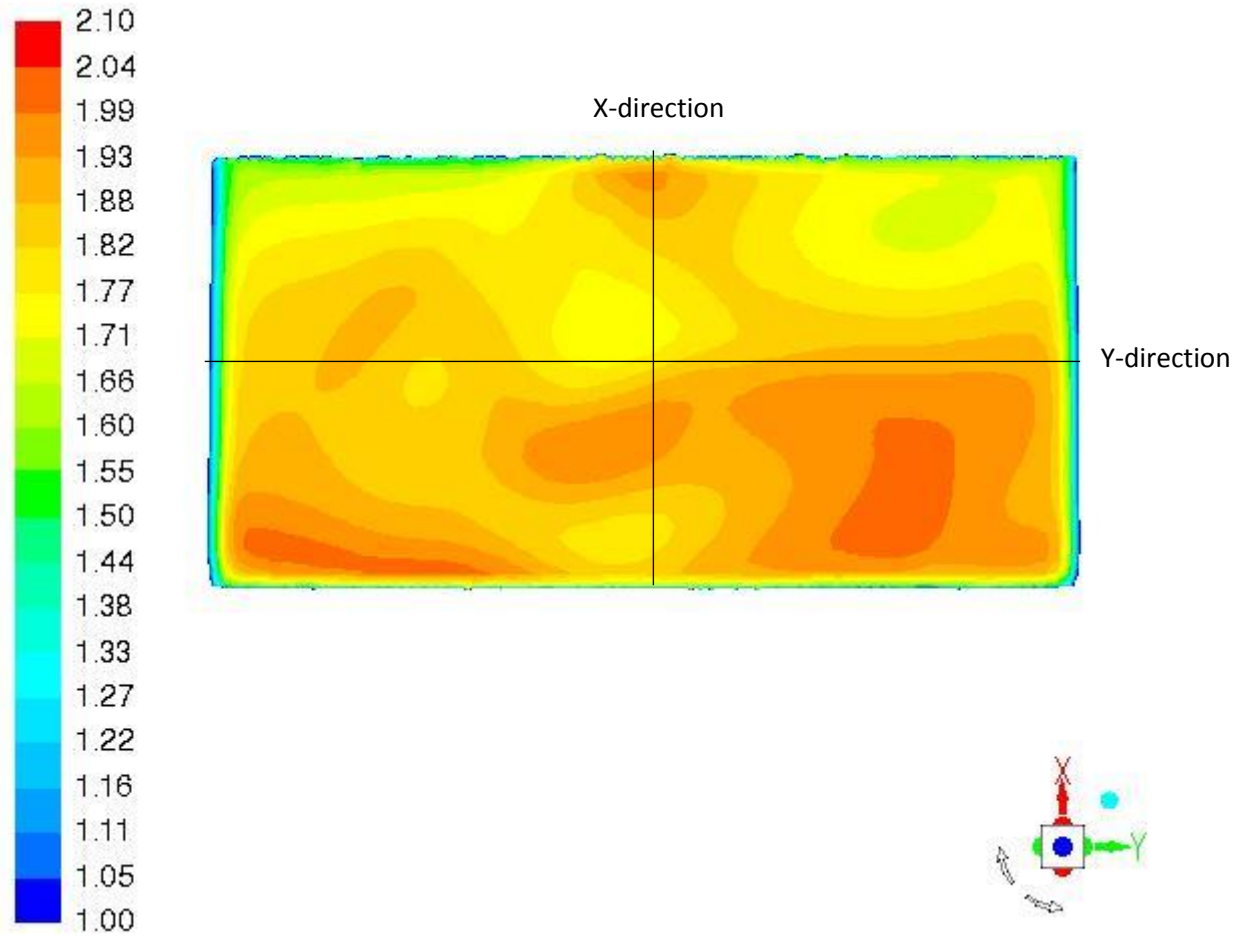

Figure 30 Full view of Z-velocity for the airflow at plane C. The black lines indicate where the velocity profiles are plotted.

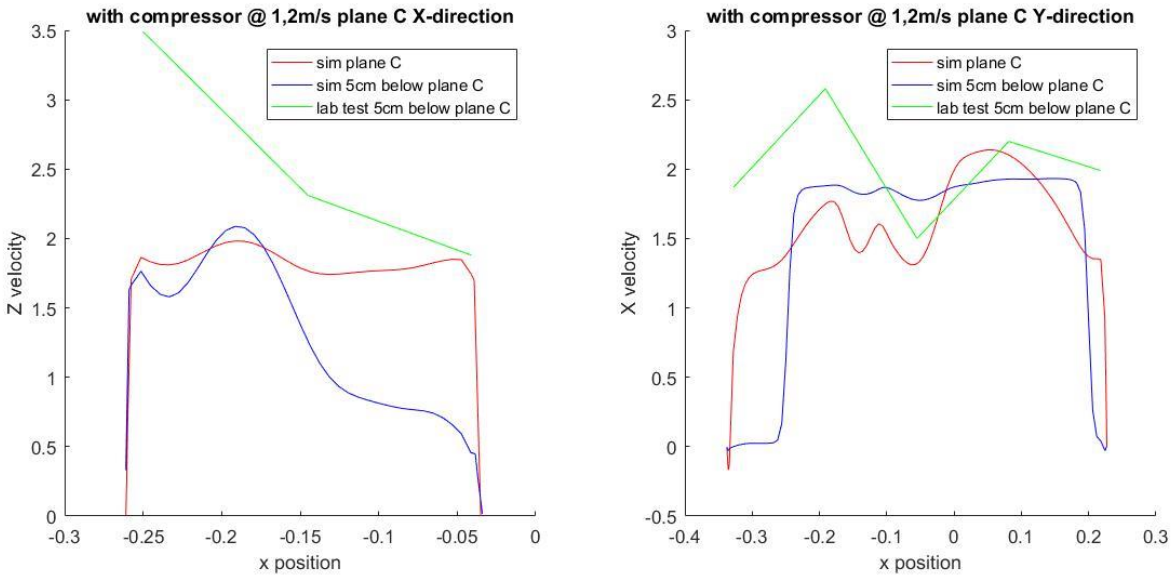

Figure 31 Z-velocity profiles along central axis in x- and y-direction. The red and blue lines are CFD results. Green line is lab measurements

3.2.6.1 Flow uniformity observations

The first thing to notice from figure 29 and 30 is that the flow is not perfectly uniform in plane C in for any of the velocity or compressor cases. The z-velocity distribution profile can be observed to follow a stable increase the further it reaches away from the inlet side in x-direction. This effect of the profile can be expected since the flow changes sharply from x- to z-direction after the inlet. What we observe is that the velocity profile has not yet recovered from this sharp bend.

However the velocity spike near the inlet side is harder to explain. To make sure this was not due to the solution being unconverged, a couple of quick controls was made:

- The Kw-SST quick run (mesh1 with less resolution to save time) was double checked on this profile plane. The same velocity spike occurs there, meaning the effect is not due to the turbulence model
- Using the coarse mesh to save time (mesh1) the profile in plane C was checked. It had the velocity spike. Then that case was set to a ten times lower residual and was further calculated (roughly 1000 iterations). The Z-velocity profiles along the line in y direction was compared and no noticeable difference was found. This proves convergence is not the reason of the velocity spike near the inlet.

The velocity spike near the inlet side was present in a case where convergence and turbulence model was checked and proved which means the velocity spike will now be trusted to not be an error. However if it is indeed an error then it is likely an effect from the mesh layout that was not identified, or it's an error in how the porous medium interacts with the regular flow geometry.

The likely explanation for the phenomenon is that the geometry narrows sharply in both sides in the y-direction for condenser (at plane C). This pushes the airflow towards the centre of the geometry. This effect also interact with the inlet being placed skewed in one y-direction and the condenser being placed skewed to the other direction. All this together was deemed the reason for the irregular profile, and the calculation result was finally trusted after this conclusion.

3.2.6.2 The CFD Velocity profile compared to locally measured lab velocities

The CFD results are more useful in giving an overview of the flow behaviour than the lab measurements of the flow behaviour. The CFD results are flexible to handle and can be plotted along any line or plane, while the lab measurements had limitations in that the instruments could not get closer than 5cm to the plane of interest. It can be observed that these 5cm allow the velocity profile to develop and change substantially in the simulation results.

The instruments connected to the Pitot static tube gave negative output values in figure 29, which was not expected. The metal traverses guaranteed that the Pitot static tubes were oriented in the correct direction, so the reason for the negative results are deemed to be the zero calibration of the digital pressure instruments connected to the pitot static tubes. Also low difference in static and dynamic pressure makes small inaccuracies in the instruments have large impact. For figure 26 it appears that all the lab values should be raised by roughly 1-2 m/s to be more reasonable. Although the lab-measurements for the velocity profiles give some unreasonable results, the general shape of their plots still matches the CFD velocity profile to some degree for all the cases (figure 29, 31, and 37 appendix A, 39 appendix B). The lab results are higher than CFD for both low velocity cases (with or without compressor), while they are lower than CFD results for both high velocity cases (with or without compressor). The reason for this strange result which seems consistent at first glance might be undetected leakages in the lab rig, or just an unlikely coincidence because the inaccurate results of the pitot static tubes for the current velocities.

3.2.6.3 Effects of the compressor

The shape of the velocity field seems constant regardless of the velocity, meaning both high and low velocity profiles with no compressor is similar (figure 28 and figure 38 appendix B). The same goes for low velocity with compressor case (figure 30) that matches high velocity with compressor case for velocity field profile (figure 36 appendix A). This indicates that the general shape of the flow remains the same for different velocities, but the compressor has some effect on the profile. It has already been proven in previous chapters that the effects are insignificant on pressure loss, but if the general velocity distribution at plane C becomes skewed from compressor influence (and thereby lowering heat pump performance) remains to be investigated in more detail in chapter 3.3.

3.2.6.4 Study of profile for outlet

In figures 32 and 33 the profile study is made at the outlet (plane E) for only a high velocity case. The air velocity is higher in this cross section so the Pitot static tubes end up giving results closer to CFD as they perform better with higher difference between static - and dynamic pressure

Plane E 2 m/s no compressor case plots

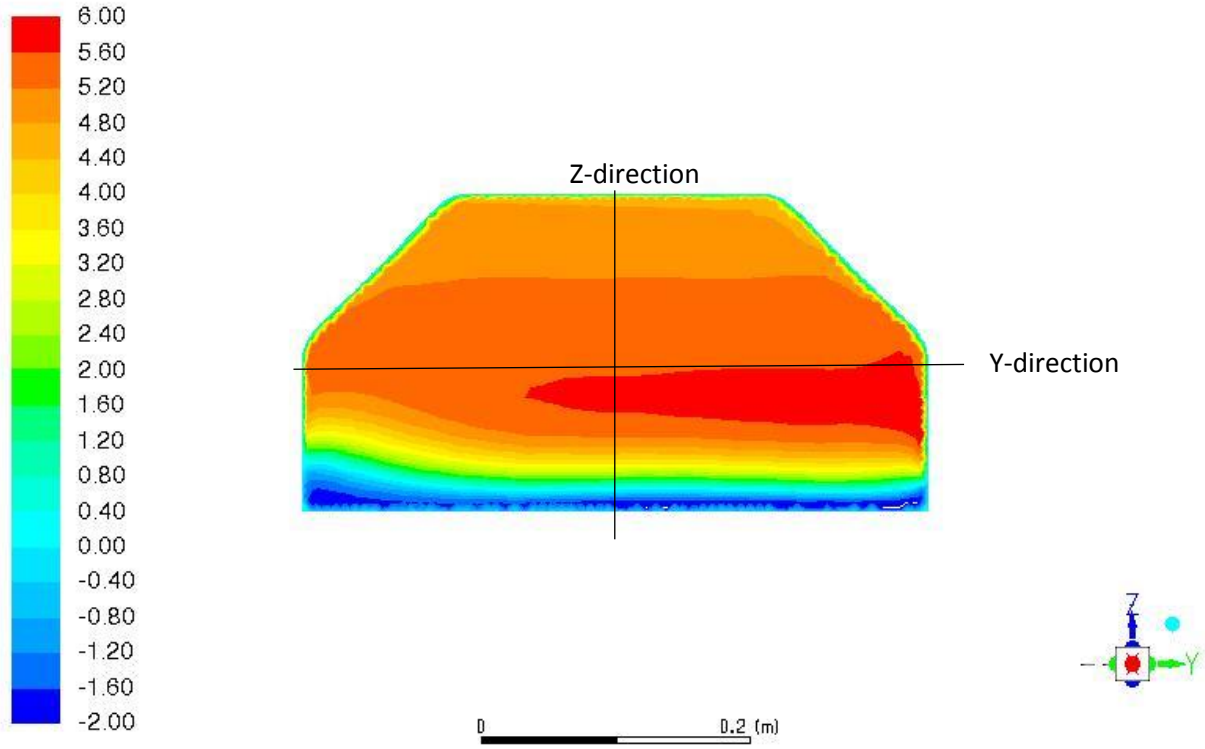

Figure 32 plane E, x-velocity distribution at the outlet.

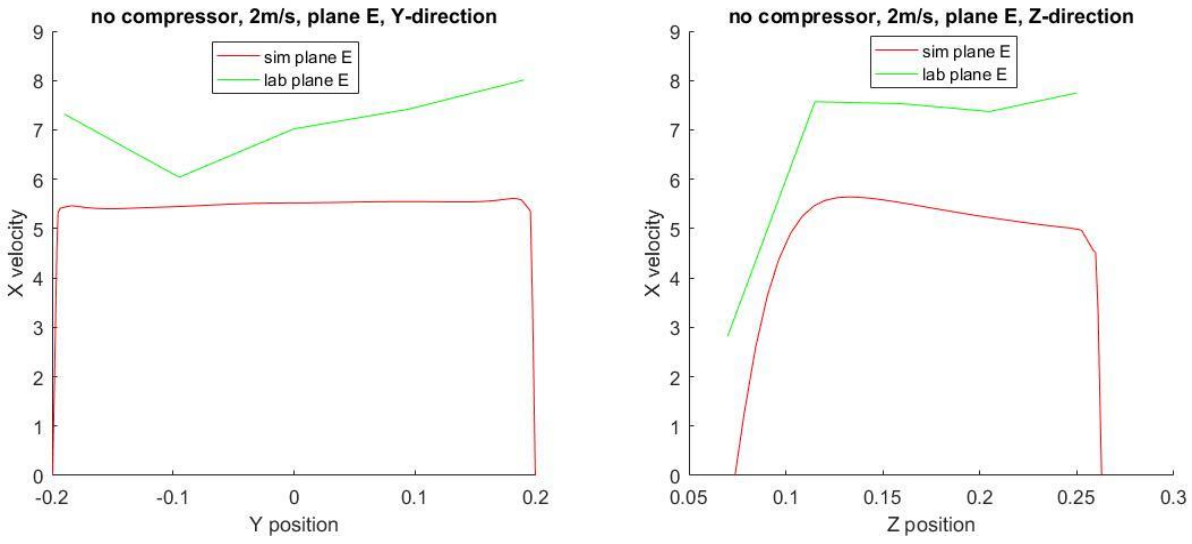

Figure 33 X-velocity at plane E (outlet) plotted for lab measurements in green and CFD results in red.

The solution looked reasonable in regard to flow uniformity. Less velocity near the sharp bend makes sense. The slight ununiformity in y-direction was deemed to be caused from the unsymmetrical placement of inlet and condenser earlier in the flow geometry.

The Pitot static tube had free space behind in the geometry so could measure at the desired points, unlike previous studies at plane C. In these curves the lab results and the simulation match well in general shape. The lab results are consistently about 2m/s too high.

Having compared all lab measurements to simulation results, conclusions can be made that there are some consistencies, but also overall differences. Most are explained by the Pitot static tube working far below their optimal range, and the measurements using traverse to get line plots at plane C and E consisting of too short data series to give an accurate value. Other possible reasons for inconsistencies could be that the porous media approximations of heat exchangers might not have been perfect, or that leakages can occur in reality but are not part of the simulation model. One advantage with CFD-results compared to lab measurements was that more varied data could be extracted with less effort than when using available lab instruments.

3.3 A closer look at the effects of removing the compressor

In figures 34 and 35, the difference in introducing the compressor is investigated closer. The plots will seem familiar but the range has been adjusted to more clearly show differences. The high velocity case was chosen, as that is the case where the turbulence effects was expected to be more significant. The goal here is to detect if the velocity distribution is less even in any of the two cases, to keep the heat exchanger working at optimum conditions.

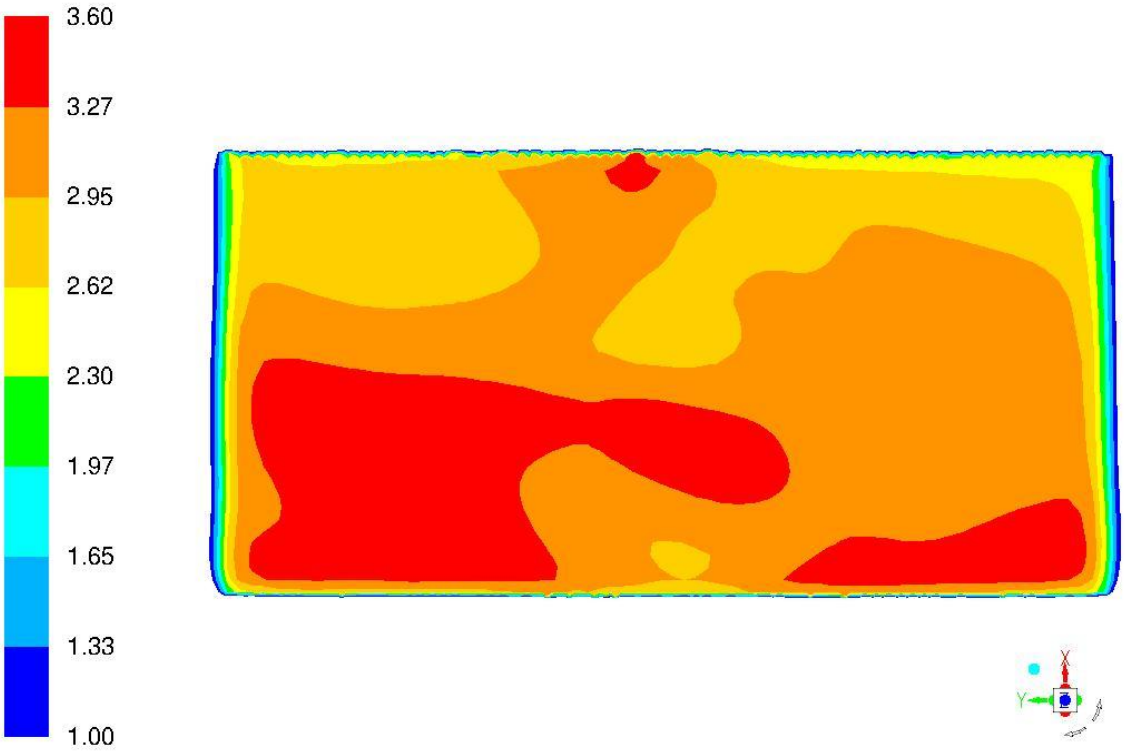

Figure 34 Full view of Z-velocity for the airflow at plane C. with compressor, high velocity.

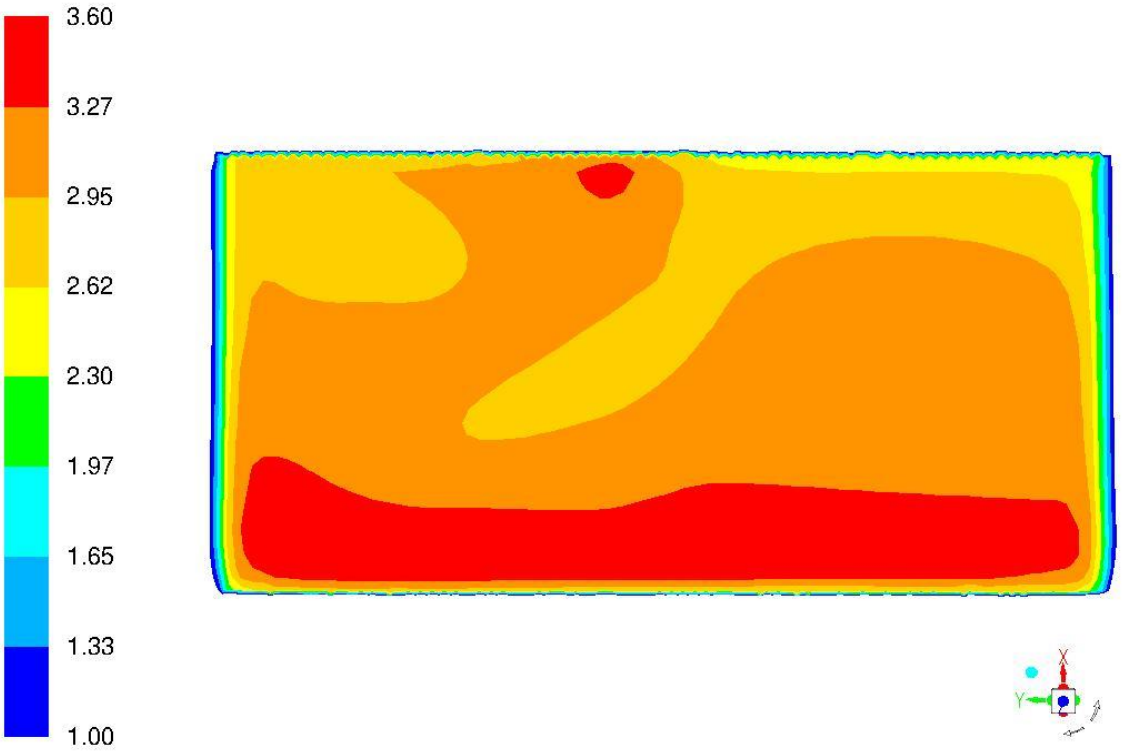

Figure 35 Full view of Z-velocity for the airflow at plane C. No compressor, high velocity.

It can be observed from figures 34 and 35 that there are some effects to the flow behaviour but just looking at the figures is not enough to decide if the difference is of relevant magnitude. To quantify the difference in how unevenly the flow is distributed, the data for all cells in plane C was post-processed in the following manner:

An average value of the z-velocity was first calculated. Then, the average deviation from the average value was calculated. The results for this is shown in table 6. To make the results less dependent of the low values close to the wall, extreme values near the wall were discarded.

Table 6 taking a cut out from plane C, where the flanks with 0 flow are discarded (as in figure 16 and 17) the cells average z velocity and the average deviation from this value was calculated. This to quantify how unevenly distributed the flow profile is at inlet to HEX 2

Plane C (2m/s)	Average Z vel. (m/s)	Average deviation (m/s)
no compressor	2.51	0.82
with compressor	2.52	0.82

Table 6 illustrates that even though a visual difference could be observed in the flow profile to the inlet of HEX2 (plane C), the overall effect appears to be insignificant down to 0.04% in how evenly the flow is distributed. This together with the earlier results in table 3 concludes that the placement of the compressor is insignificant to any effects of the pressure losses or flow distribution to the HEX2.

3.4 Final discussion of the pressure loss distribution in the heat pump side based on simulation results.

As the empty spaces between the components are the ones that have a potential to be aerodynamically optimized, it's of interest to investigate how large part of the overall system pressure loss that comes from those parts of the geometries. This quantity is plotted in table 7. The total system pressure losses come from the theoretical Matlab model.

Table 7 - This table illustrates how large part of the entire system load is caused by different zones, based on simulation result for 2m/s with compressor case. This case is with no filter clog and no drum load, meaning the empty spaces will theoretically never have as much relative impact as this case. If these areas are optimized, these load values are the maximum efficiency gain for the perfect case.

with compressor 2 m/s	CFD	CFD	CFD	CFD	Theoretical model	Theoretical model
planes	A-B	B-C	C-D	D-E	Drum and filter	total for system
	HEX1	Empty space	HEX2	empty space		
Pa	30.9	11.0	272	19.2	257	590
% system	5%	2%	46%	3%	44%	100%

It can be observed that the empty areas between planes B-C and D-E (those are between HEX1 and HEX2) only have an impact of 5% of the whole system. If load is introduced this % would go down further. Removing the compressor had an insignificant effect to the pressure losses, but from previous studies investigated it had been found a case where a local improvement reduced local pressure loss in an empty space by 23% on another tumble dryer. Zones between plane B-C and D-E can be optimized, in particular by rounding the sharp bends at the inlet and outlet as observed when figure 21-26 was studied. If they are at this optimized state, the gains would never be more than 5% reduced pressure loss.

4 Conclusions

4.1 The theoretical model

A prototype for a theoretic model of the pressure distribution across the whole air flow system for this specific model of heat pump tumble dryer was completed. The geometry was deemed too complicated for any predefined pressure loss functions to be used for any components, and pressure distribution functions were instead found using a manual iterative process based on lab data collected for static pressure and volume flow measured at the laboratory in Ljungby. Inputs for the model was laundry load of 0-20kg and filter clogging of 0-90% and the output was gauge pressure throughout the system. To keep the model from being too difficult to construct, variables like temperature, heat transfer, humidity, leakage and drying time was not investigated and set to constant conditions when needed.

Overall pressure loss for the system and the average gauge pressure for the system could be modelled using simple polynomial functions. At that stage it was deemed possible to design modelling tools using some kind script to test different degrees of polynomial functions until acceptable accuracy is achieved, using lab data as input. However when the load distribution across the different component was introduced, it was hard to find any simple consistent solution that could give any accurate modelling of the results measured from the laboratory.

The method for building these functions was generally finding how the pressure varied for filter clogging while keeping load constant at 0. Then as the initial values of pressure had been modelled, the functions were expanded to include both varying filter clogging and loads.

The theoretical model prototype was found useful in finding critical loads or filter clogging degrees where suction was lost in the drum, and a fully loaded drum could be observed to reach rapidly declining performance as filter clogged 70% and upwards.

4.2 The CFD flow computations

The heat pump side of the geometry could be successfully modelled and investigated. The main challenge was to model the two heat exchangers and a porous medium method was used, which had its resistance coefficients calibrated from lab measurements of pressure (99.7% accurate) and velocity (98.5% accurate) for a low load case. When changing to a high load case with the inlet velocity from 2m/s to 1.2m/s (98.8% close to CFD) the pressure was over estimated by CFD model by 23.8% compared to lab measurements. That means the porous model of the heat exchangers was successful but there is room to improve calibrations based on a lab measurements for a wider span of velocity cases (see chapter 3.2.3 for these results).

Some wake regions (stalled velocity) was identified using visual study of the CFD results. These created turbulent pressure losses and were concentrated at the 90˚ sharp turn at the inlet and at the outlet. The quantity of all pressure losses in the regions outside of the heat exchangers was 10.9 Pa and 19.18 Pa for the low load, high velocity case.

The CFD results indicate that there is more potential gain from optimising losses in heat exchanger 2 than in the empty spaces around it.

In general pitot static tubes was successful in measuring static pressure for calibrating the CFD model and the heat exchangers. But the suggested method to post validate the CFD results with pitot tubes to measure difference in static and dynamic pressure was not useful, as the low difference in pressure left the measurement instrument too inaccurate. The pitot tubes also had some issues with space limitations to measure velocity close to the inlet of the condenser.

4.3 The geometry improvement investigation

The compressor was investigated to find if it had any impact on pressure loss or velocity distribution for the condenser. Both lab measurements and CFD results show that the compressor was insignificant for both velocity distribution with 0.04% different in unevenness at the inlet to condenser (chapter 3.3) and pressure losses 1-3% of the heat pump side (chapter 3.2.3). CFD estimated slightly higher differences than lab results but this was likely an effect of the simple geometry approximation for the compressor as cylinders with sharp edges. The CFD can be expected to overestimate effects of compressor slightly because of these geometry approximations.

It was intended to compare CFD velocity profiles to lab measurements at the same locations. The velocity profiles did match the velocity measured in the lab to some degree in general shape of the profiles. The velocities did not match quantitatively though. These differences were deemed to mostly come from inaccuracies in Pitot static tube measurements rather than errors in the CFD model. This was particularly true for low velocities at the inlet to the condenser. See chapter 3.2 for further details in this subject.

4.4. Suggestions for future studies

The theoretical model can be improved in several ways. The current model only works for one tumbler configuration with load and filter clogging as inputs, but it could be attempted to calibrate it

for more configurations and spectrum of components. Leakage can be included, as can heat transfer, multiphase flow (humidity), and the model could be made transitional to account for drying time.

If more lab tests are performed for future calibration, the filter clogging degree could be modelled more realistically using varying perforated plates. Pitot static tubes were inaccurate in describing the low velocities. Heat wire measurements or optical studies could be used as a measuring method instead.

For the CFD study, multi-phase and heat transfer and a transient case could be run. This could be used to help study drying times.

The modelling of a heat exchanger as a porous medium was deemed possible in this thesis, and the process could be refined. The calibration could be made for multiple cases, and the load coefficients for the porous medium could be modelled as functions of the inputs.

The heat pump side for the airflow was studied in this thesis. A CFD study could be made of the remainder of the system geometry, such as drum, filter and fan. The filter could probably also be modelled as a porous medium as mentioned in the literature study chapter 1.1.4 [6].

Other geometrical improvements focusing more on the shell of the geometry instead of the compressor could be performed. As mentioned in the visual overview of the flow chapter 3.2.4, there are some unwanted wake regions forming close to the sharp bends of the inlet and outlet. The empty spaces have a pressure loss of up to about 30Pa (table 7 in chapter 3.4) out of the whole system (minimum 590Pa) (table 7 in chapter 3.4). When comparing with the literature study, some smoothing of edges reduced local pressure losses by 23% [6], so a similar gain could likely be made for this tumble dryer.

5 Bibliography

[1] Crook, Austin Winkelman, “Modeling and design of a high efficiency hybrid heat pump clothes dryer”, Applied Thermal Engineering, Volume 124, September 2017, Pages 170-177

[2] Payam Nejat et al., “A global review of energy consumption, CO2 emissions and policy in the residential sector (with an overview of the top ten CO2 emitting countries)”, Renewable and Sustainable Energy Reviews, Volume 43, March 2015, Pages 843-862

[3] Manuel R. Conde, “Energy conservation with tumbler drying in laundries”, Applied Thermal Engineering, Volume 17, Issue 12, December 1997, Pages 1163-1172

[4] Li Chunxi, Wang Song Ling, Jia Yakui,” The performance of a centrifugal fan with enlarged impeller”, Energy Conversion and Management, Volume 52, Issues 8–9, August 2011, Pages 2902-2910

[5] Torrano, I. Martinez-Agirre, M. Tutar, M. “Numerical characterization of pressure drop through a low speed wind tunnel: Some design aspects”, 2013 International Renewable and Sustainable Energy Conference (IRSEC) Renewable and Sustainable Energy Conference (IRSEC), 2013 International. :240-245 Mar

[6] Kamal Rezk, Jan Forsberg, “Geometry development of the internal duct system of a heat pump tumble dryer based on fluid mechanic parameters from a CFD software”, In Applied Energy 2011 88(5):1596-1605

[7] Xiaolong Zhang, Peichi Tseng, Muhammad Saeed, Jiyang Yu, “A CFD-based simulation of fluid flow and heat transfer in the Intermediate Heat Exchanger of sodium-cooled fast reactor”, In Annals of Nuclear Energy November 2017 109:529-537

[8] Erik Ingelstam, Rolf Rönngren, Stig Sjöberg, “Tefyma”, third edition, Studentlitteratur AB Lund, 2012

[9] 2009 Ansys Fluent *User’s Guide*, http://users.ugent.be/~mvbelleg/flug-12-0.pdf, accessed 20/12-2017

6 Appendix A

Plane C 2 m/s with compressor case

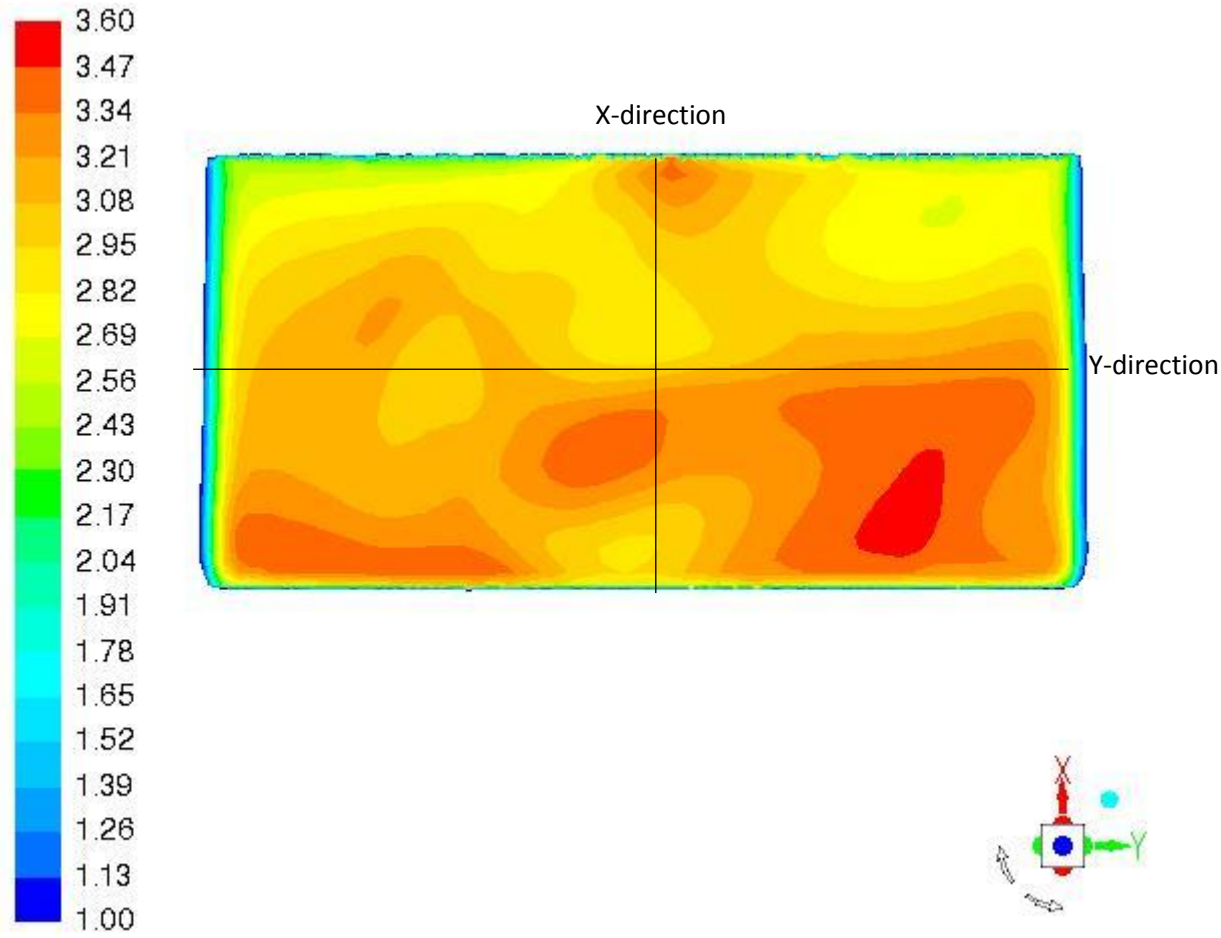

Figure 36 Full view of Z-velocity for the airflow at plane C. The black lines indicates where the velocity profiles are plotted.

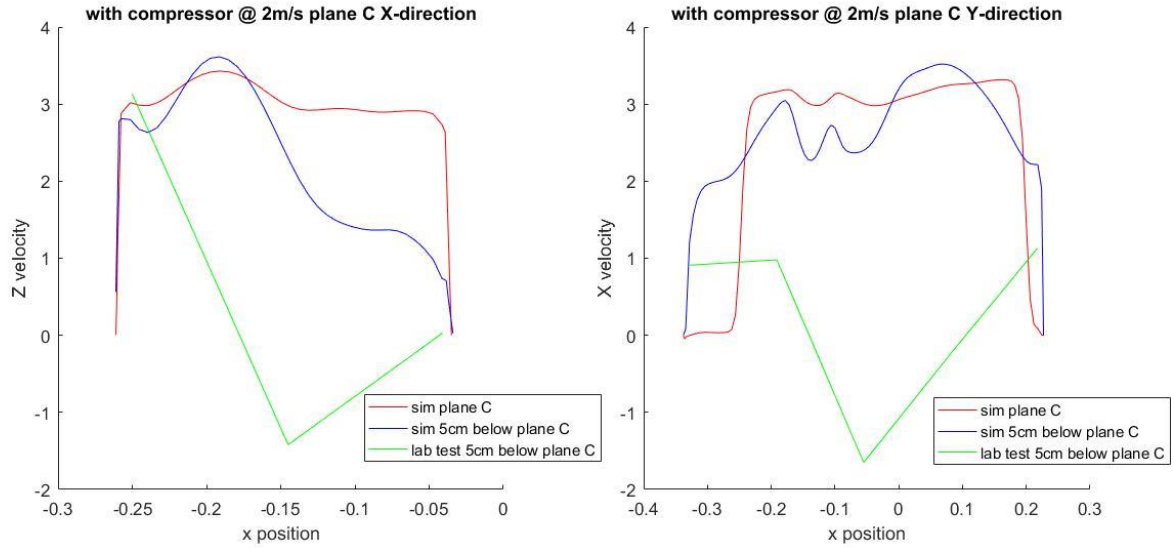

Figure 37 Z-velocity profiles along central axis in x- and y-direction. Red and blue lines are lab results. Green line is lab measurements

7 Appendix B

Plane C 1.2 m/s no compressor case

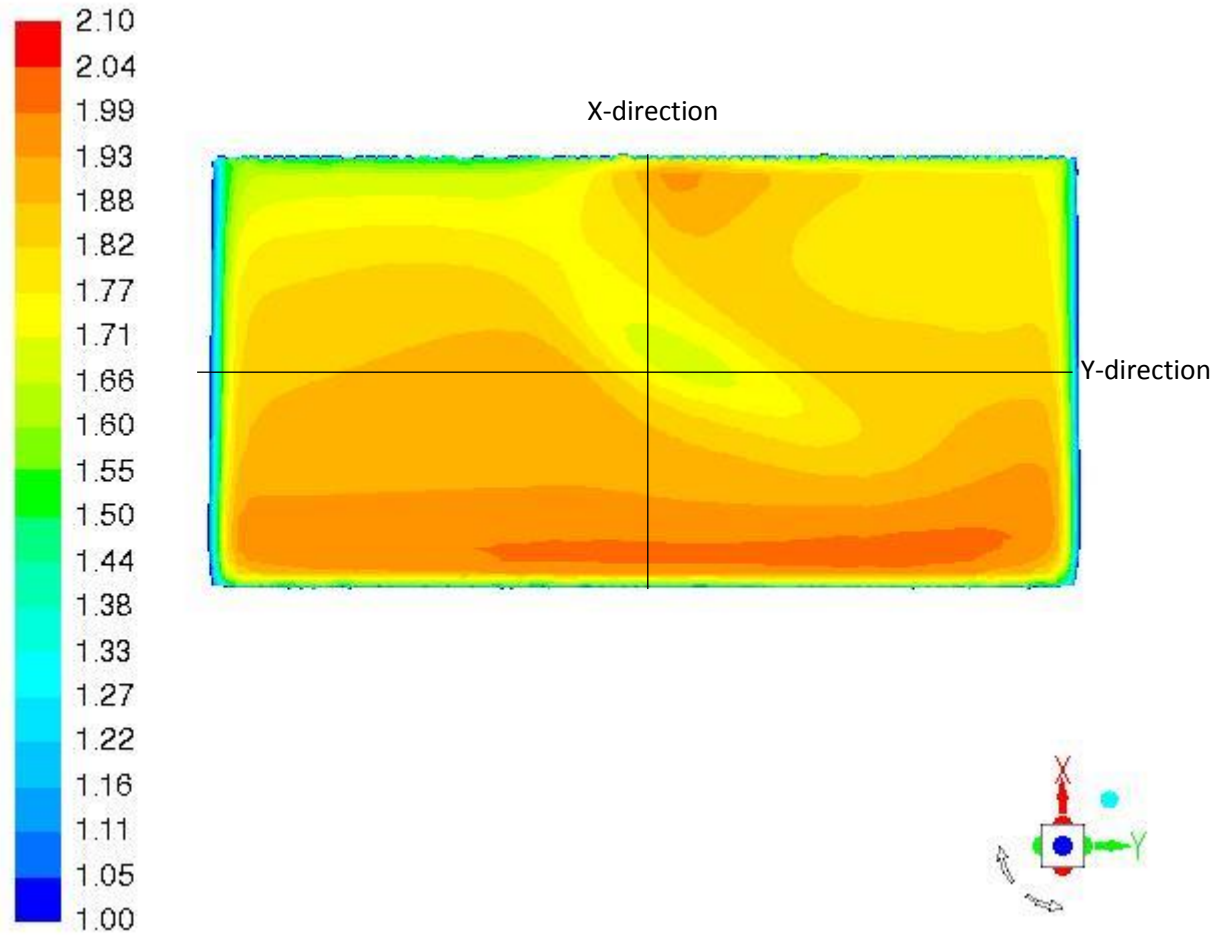

Figure 38 Full view of Z-velocity for the airflow at plane C. The black lines indicates where the velocity profiles are plotted.

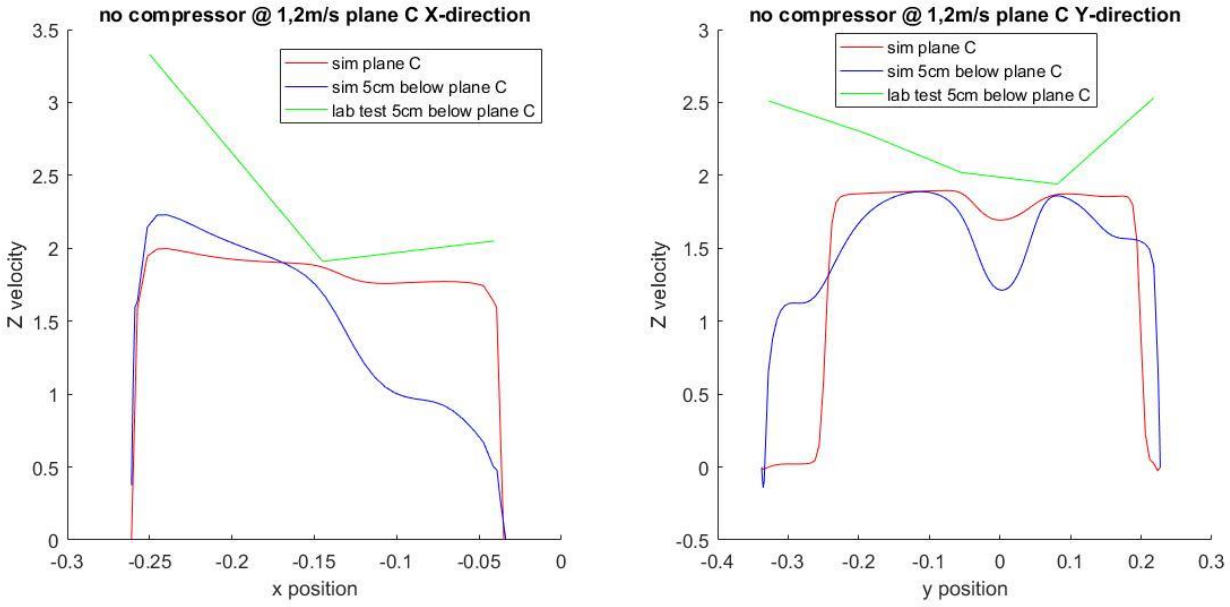

Figure 39 Z-velocity profiles along central axis in x- and y-direction. Red and blue lines are lab results. Green line is lab measurements